Molecular Therapy
Nucleic Acids
Original Article

miR-199a-3p increases the anti-tumor activity of palbociclib in liver cancer models

Elisa Callegari,[1,6] Paola Guerriero,[1,2,6] Cristian Bassi,[1,2] Lucilla D'Abundo,[1] Antonio Frassoldati,[1] Edi Simoni,[3] Laura Astolfi,[3] Enrico Maria Silini,[4] Silvia Sabbioni,[2,5] and Massimo Negrini[1,2]

[1]Department of Translational Medicine, University of Ferrara, Via Luigi Borsari, 44121 Ferrara, Italy; [2]Laboratorio Per Le Tecnologie Delle Terapie Avanzate (LTTA), Department of Translational Medicine, University of Ferrara, 44121 Ferrara, Italy; [3]Bioacoustics Research Laboratory, Department of Neurosciences, University of Padua, 35129 Padua, Italy; [4]Section of Anatomy and Pathology, University Hospital of Parma, 43121 Parma, Italy; [5]Department of Life Sciences and Biotechnology, University of Ferrara, Via Luigi Borsari, 44121 Ferrara, Italy

Palbociclib is in early-stage clinical testing in advanced hepatocellular carcinoma (HCC). Here, we investigated whether the anti-tumor activity of palbociclib, which prevents the CDK4/6-mediated phosphorylation of RB1 but simultaneously activates AKT signaling, could be improved by its combination with a PI3K/AKT/mTOR inhibitor in liver cancer models. The selective pan-AKT inhibitor, MK-2206, or the microRNA-199a-3p were tested in combination with palbociclib in HCC cell lines and in the TG221 HCC transgenic mouse model. The combination palbociclib/MK-2206 was highly effective, but too toxic to be tolerated by mice. Conversely, the combination miR-199a-3p mimics/palbociclib not only induced a complete or partial regression of tumor lesions, but was also well tolerated. After 3 weeks of treatment, the combination produced a significant reduction in number and size of tumor nodules in comparison with palbociclib or miR-199a-3p mimics used as single agents. Moreover, we also reported the efficacy of this combination against sorafenib-resistant cells *in vitro* and *in vivo*. At the molecular level, the combination caused the simultaneous decrease of the phosphorylation of both RB1 and of AKT. Our findings provide pre-clinical evidence for the efficacy of the combination miR-199a-3p/palbociclib as anti-HCC treatment or as a new approach to overcome sorafenib resistance.

INTRODUCTION

Hepatocellular carcinoma (HCC) comprises 80% of primary liver cancers and is the fourth-leading cause of cancer deaths worldwide.[1] Advanced-stage HCC exhibits a poor prognosis. Among treatments for advanced HCC, the multikinase inhibitor sorafenib has been the only therapeutic option available for more than 10 years. More recently, additional small molecules, such as lenvatinib, have been approved for first-line HCC treatment, while second-line therapy options include regorafenib and cabozantinib.[2] The immune-checkpoint inhibition has recently expanded the treatment landscape for advanced HCC and the combination of atezolizumab (anti-PDL1 antibody) and bevacizumab (anti-VEGF antibody) was the first regimen to improve overall survival compared with sorafenib.[3] Other molecules, such as CDK4/6 inhibitors (e.g., palbociclib, ribociclib), are in earlier stages of clinical testing.[4]

The use of palbociclib was granted for clinical use in 2015 in combination with letrozole for the treatment of postmenopausal women with estrogen receptor (ER)-positive, HER2-negative advanced breast cancer,[5] and in 2016 in combination with fulvestrant for the treatment of women with hormone receptor (HR)-positive, HER2-negative advanced or metastatic breast cancer with disease progression following endocrine therapy.[6] In patients with advanced HCC, a phase II trial is currently active to determine whether palbociclib can be effective in subjects with inoperable, recurrent/refractory, advanced HCC who failed or are intolerant to standard first-line therapy with sorafenib[7] (ClinicalTrials.gov Identifier: NCT01356628).

Palbociclib is a selective CDK4/6 inhibitor that efficiently blocks cell cycle progression by preventing the CDK4/6-mediated phosphorylation of RB1.[8] While known to be effective in RB1-proficient cells, palbociclib was also shown to be active on tumor cell lines independently of RB1 gene status by inhibition of FOXM1 phosphorylation.[9] Oddly, palbociclib was shown to induce a dose-dependent up-regulation of MTOR and AKT protein phosphorylation, leading to the activation of AKT signaling[10] and potentially reducing its anti-tumor efficacy. This finding provides a rationale for the use of palbociclib in combination with inhibitors of the PI3K/AKT/MTOR pathway. Indeed, the combination of palbociclib with PI3K/MTOR/AKT inhibitors was shown to potentiate the pro-apoptotic effect in triple-negative breast cancer cells[11] and in malignant pleural mesothelioma cells.[12]

Here, we investigated whether the combination of palbociclib with agents active on AKT could be effective on liver cancer. In cellular and *in vivo* HCC models, palbociclib was combined with MK-2206, a selective pan-AKT inhibitor, whose anti-cancer activity was

Received 22 November 2021; accepted 15 July 2022;
https://doi.org/10.1016/j.omtn.2022.07.015.

[6]These authors contributed equally

Correspondence: Silvia Sabbioni, Department of Life Sciences and Biotechnology, University of Ferrara, Via Luigi Borsari, 46 - 44121 Ferrara, Italy.
E-mail: silvia.sabbioni@unife.it
Correspondence: Massimo Negrini, Department of Translational Medicine, University of Ferrara, Via Luigi Borsari, 46 - 44121 Ferrara, Italy.
E-mail: massimo.negrini@unife.it

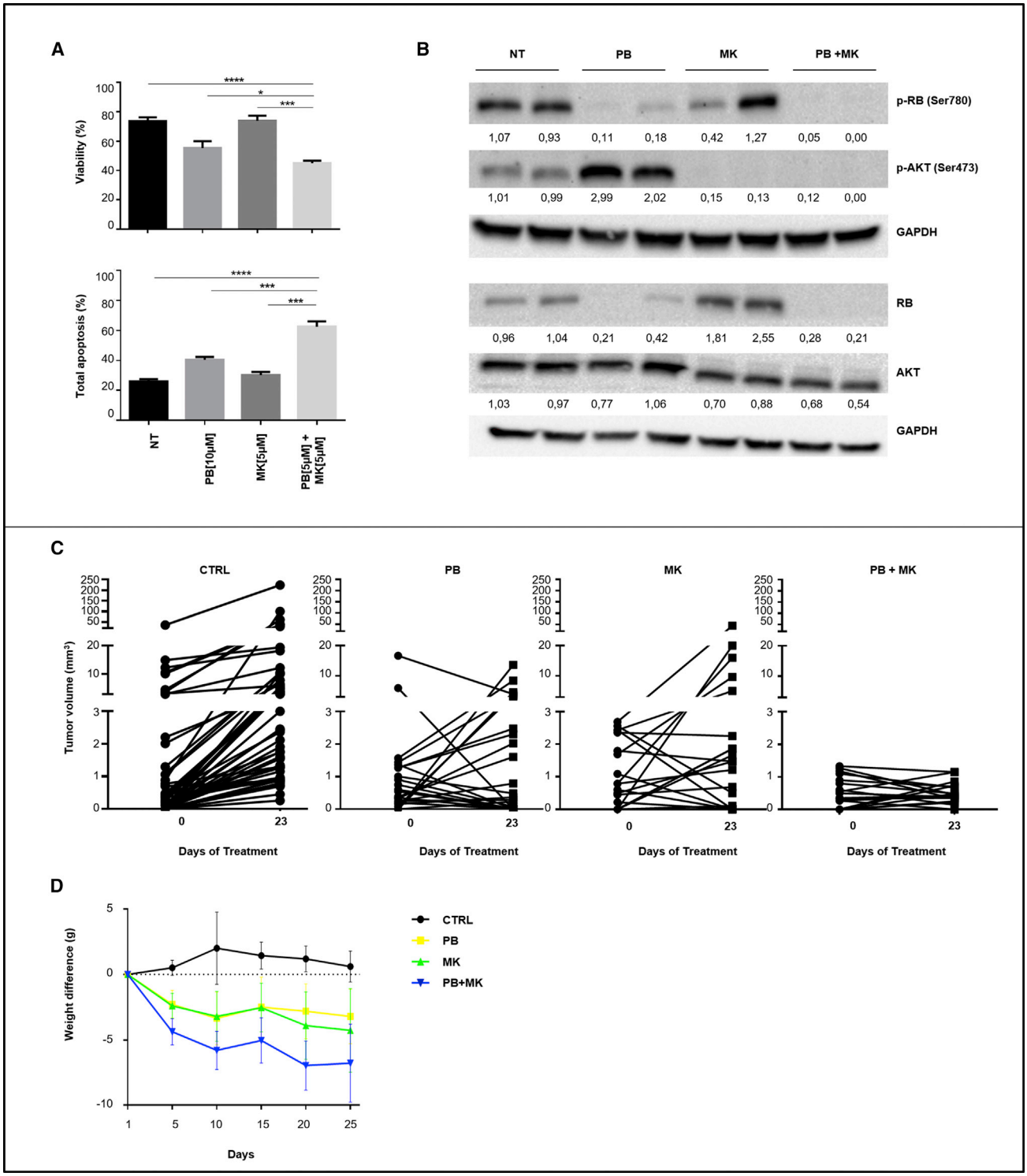

Figure 1. The combination of AKT and CDK inhibitors is effective against HCC cells

(A) HepG2 cells were treated with palbociclib (PB) (10 μM) or MK-2206 (MK) (5 μM) as single agents or with the combination of the two (PB 5 μM + MK 5 μM). A fourth group of cells received no treatment (NT). Viability and apoptosis were evaluated 72 h after the beginning of treatment. Data are represented as mean ± SD. *p value ≤0.05; **p value ≤0.01; ***p value ≤0.001; ****p value ≤0.0001. (B) Western blot analysis and quantification of RB1, AKT proteins and their phosphorylated forms in

(legend continued on next page)

demonstrated in both pre-clinical settings and clinical trials,[13,14] or with miR-199a-3p, which was shown to modulate MTOR and PAK4 oncoproteins, both essential factors of the PI3K-AKT-PTEN molecular pathway.[15-18] miR-199a-3p, a microRNA (miRNA) down-regulated in virtually all HCCs,[19] was associated with poor survival in HCC patients. Restoration of miR-199a-3p was shown to exhibit a significant anti-tumor activity in experimental models.[15,19-22] It was also shown to enhance doxorubicin sensitivity in HCC cells, suggesting a potential strategy for increasing HCC chemosensitivity, but no correlation was found with sorafenib resistance.[23-27]

RESULTS

Increased efficacy of palbocicib on HCC *in vitro* and *in vivo* by combination with the AKT inhibitor MK-2206

We investigated the effects of palbociclib and MK-2206, either as single agents or as combination on human HepG2 and Hep3B liver cancer cells. Compared with single drugs, the combination induced a significant increase in apoptosis in HepG2 cells (Figure 1A). A significant reduction of palbociclib IC50 was detected when used in combination with MK-2206 (Figure S1). At the molecular level, palbociclib as single agent induced a decrease of phosphorylated RB1 protein and, at the same time, an increase of AKT phosphorylation (residue S473). In addition, we also observed a reduction of total RB1protein, as typically described for palbociclib in other reports.[8] Instead, MK-2206 as single agent, inhibited the phosphorylation of AKT at residue S473. When combined, the two drugs produced a simultaneous decrease in p-RB1 and p-AKT (Figure 1B).

The combination produced the same biological effects in Hep3B cells (Figure S2A). However, since Hep3B cells carry an STOP codon in the *RB1* gene (c.1727C>G, p.Ser576Ter), a very low expression of full-length RB1 protein can be found in these cells (Figure S3). This finding suggests that inhibition of RB1 protein phosphorylation is unlikely a major mechanism responsible for the observed pro-apoptotic effects of palbociclib on Hep3B cells. Hence, we investigated and confirmed that palbociclib induced an inhibition of FOXM1 activity mainly by reducing total FOXM1 protein (Figure S2B), as also previously reported.[9,28] As FOXM1 activation is AKT-dependent,[29,30] inhibition of FOXM1 was also sustained by MK-2206 (Figure S2B).

The *in vitro* results prompted us to investigate the *in vivo* anti-cancer activity of palbociclib and MK-2206. TG221 male mice were treated intraperitoneally (i.p.) with the carcinogen N-diethylnitrosoamine (DEN) at 10 days of age to accelerate the development of liver tumors. Tumor development was monitored by ultrasonography. When the volume of tumors reached about 2 to 3 mm^3, at approximately 6 months of age, mice were split into four experimental groups: (1) palbociclib (100 mg/kg); (2) MK-2206 (150 mg/kg); (3) palbociclib (100 mg/kg) + MK-2206 (150 mg/kg); and (4) vehicle. Each drug was daily administered by oral gavage for 3 weeks (21 days). Drug efficacy was assessed by measuring tumor nodule volumes by ultrasonography at the beginning and at the end of the treatment. Single agents exhibited heterogeneous effects, ranging from complete response to no response on single nodules. The combination produced either a complete response or stable disease, with no obvious progression (Figures 1C and Table S1), but it was hardly tolerated as shown by the substantial weight loss of all mice in the combination treatment arm (Figure 1D).

Anti-tumor activity of palbociclib was enhanced by miR-199a-3p

Since we have previously shown that miR-199a-3p can act on AKT activation,[15] we tested the *in vitro* and *in vivo* efficacy of the combination palbociclib + miR-199a-3p. The expression levels of miR-199a-3p in the different cell lines employed in the study are shown in Figure S4. They all exhibit very low levels of miR-199a-3p expression.

We first investigated the *in vitro* effects of palbociclib and miR-199a-3p either as single agents or as combination on human HCC cells. Hep3B cells were transduced with an adeno associated viral vector expressing miR-199a-3p (AAVV-199) at an MOI = 100 (Figure 2A) and treated with palbociclib (20 μM). The combination led to a decrease in viability and a higher level of cell apoptosis than single agents or control AAVV (AAVV-CTRL) (Figure 2B). Identical effects were also observed in HepG2 cells (Figures S5A and S5B). At the molecular level, the combined administration of miR-199a-3p and palbociclib led to a reduction of the phosphorylated AKT (S473), decreasing the activation of AKT induced by palbociclib in both cell lines (Figures 2C and S5C). Also in this case, analysis of FOXM1 in Hep3B cells revealed a reduction of phosphorylation and amount of FOXM1 protein in samples treated with palbociclib, both as a single agent and in combination with miR-199a-3p (Figure 2C). As FOXM1 activation is also AKT-dependent,[29,30] inhibition of FOXM1 was also mediated by miR-199a-3p, as we previously reported[15](Figure 2C).

Then, we investigated the effects of the mir-199a-3p and palbociclib combination *in vivo* (Figures 2D–2F). As in the previous experimental setting, at time of appearance of tumor nodules, mice were randomly split into the following groups: (1) palbociclib (100 mg/kg); (2) miR-199a-3p mimics (5 mg/kg); (3) palbociclib (100 mg/kg) + miR-199a-3p mimic (5 mg/kg); and (4) vehicle/scramble oligonucleotides. As an additional control, a group of animals treated with sorafenib was included. miRNA mimics were administered by i.p. injection three times a week, while palbociclib or sorafenib drugs were administered by daily oral gavage, for 3 weeks (21 days). Tumor volume was monitored by ultrasonography at the beginning and at the end of treatment, showing the growth trend of tumor nodules: the

HepG2-treated cells. The values are normalized on the GAPDH protein levels. (C) Tumor nodule volumes in DEN-treated TG221 mice of the following groups: (1) palbociclib (PB) (n = 6); (2) MK-2206 (MK) (n = 6); (3) palbociclib + MK-2206 (PB + MK) (n = 5); (4) vehicle (CTRL) (n = 13). Experimental therapies started at 6 months, when all mice presented one or more tumor nodules in their livers. Single tumor nodules were monitored by ultrasound at the beginning and end of treatment. (D) Mice weight was monitored during treatment to check drug toxicity. Data are represented as mean ± SD.

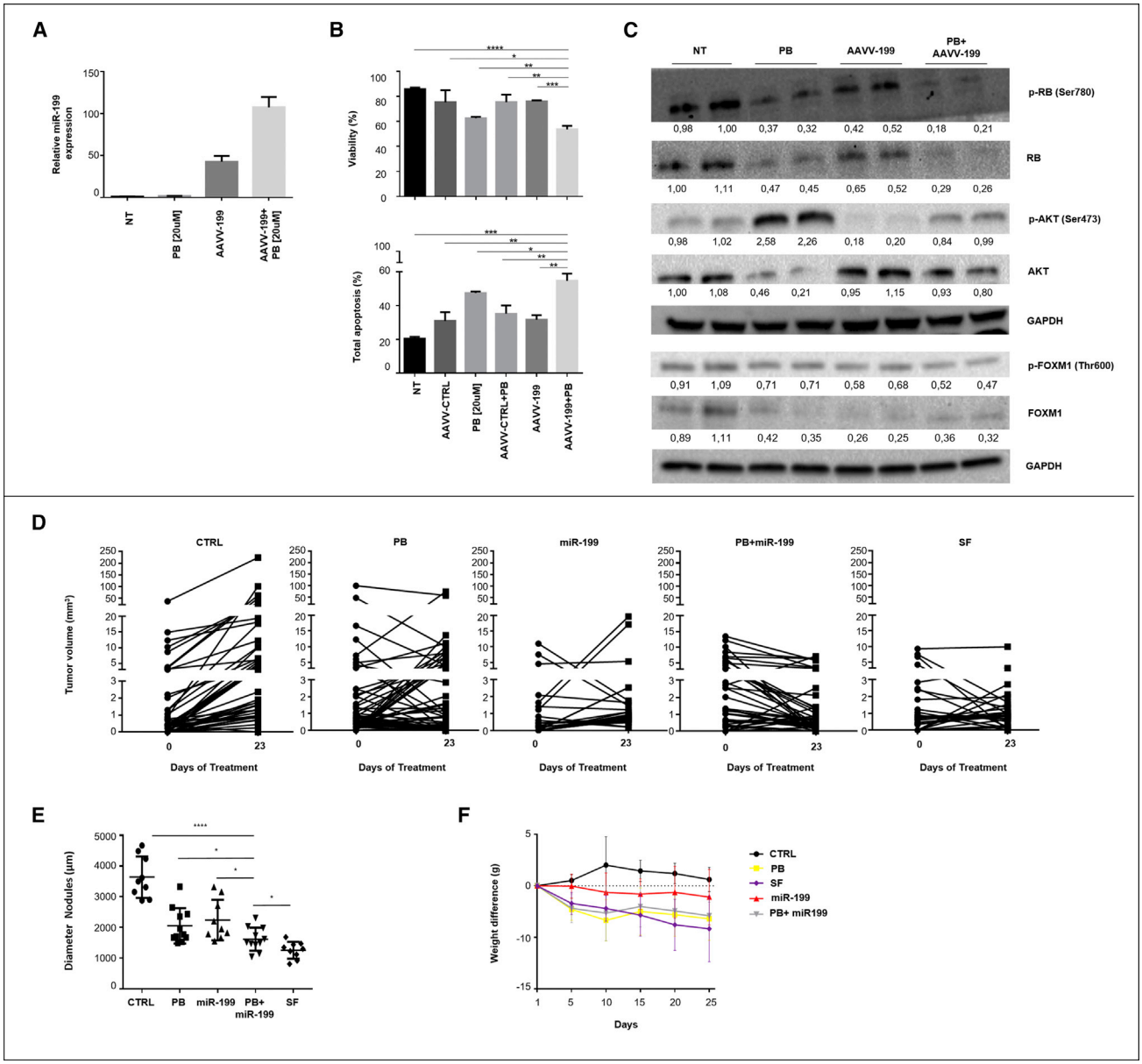

Figure 2. miR-199a-3p increased palbociclib efficacy on human HCC cells *in vitro* and *in vivo*

(A) Hep3B cells were transduced with an Adeno Associated Virus expressing miR-199a-3p (AAVV-199) or with a control AAV (AAVV-CTRL) at MOI = 100. A group of cells received no treatment (NT). Palbociclib (PB) (20 μM) was added to cell culture 72 h before cell collection. The levels of miR-199a-3p were measured 120 h after transduction. (B) Viability and apoptosis were evaluated 120 h after transduction. Data are represented as mean +SD. (C) Western blot analysis and quantification of RB1, AKT, FOXM1, and their phosphorylated forms in Hep3B-treated cells. The values were normalized on the GAPDH expression. Because Hep3B cells exhibit a low level of full-length protein, digital images of RB1 and p-RB1 were acquired with an exposure time of 300 s instead of 30 s. (D) Tumor nodule volumes in DEN-treated TG221 mice of the following groups: (1) palbociclib (PB) (n = 11); (2) miR-199a-3p mimics (miR-199) (n = 9); (3) palbociclib + miR-199a-3p mimics (PB + miR-199) (n = 11); (4) sorafenib (SF) (n = 9); (5) vehicle/scramble oligonucleotides (CTRL) (n = 9). Experimental therapies started at 6 months, when all mice presented one or more tumor nodules in their livers. Single tumor nodules were monitored by ultrasound at the beginning and end of treatment. (E) Distribution of tumor nodule size measured at the time of euthanization. (F) Mice weight was monitored during treatment to check drug toxicity. Data are represented as mean ± SD. *p value ≤0.05; **p value ≤0.01; ***p value ≤0.001; ****p value ≤0.0001.

combination was superior to the single agents and not inferior to sorafenib (Figure 2D and Table 1). Mice treated with the combination of palbociclib and miR-199a-3p showed a reduction of tumor growth and regression of some nodules, as confirmed by the significant reduction in size of tumor lesions in comparison with single agents or untreated controls at time of euthanization (Figure 2E). An

Table 1. *In vivo* anti-cancer activity of palbociclib and mir-199a-3p

	N of mice	Increase of tumor volume between post and pre-treatment (mean ± SD, mm^3)
CTRL	9	11.30 ± 30.90
PB	11	0.69 ± 12.50
PB + miR199	11	−1.62 ± 2.90
SF	9	−0.43 ± 2.13
miR199	9	1.29 ± 5.45

CTRL = untreated; PB = palbociclib; SF = sorafenib.

increase of apoptosis and a decrease of cell proliferation were detected in mice treated with miR-199a-3p and palbociclib combination in comparison with single agents or untreated controls (Figures S6A and S6B). Considering that TG221 mice are immunocompetent, we evaluated the presence of lymphocytic infiltrates that could have influenced the results. No or very little immune or inflammatory component was detected in tumor lesions, indicating that the anti-tumor effect of miR-199a-3p with palbociclib was not mediated or sustained by an immune response (Figure S7). All treatments were well tolerated by animals, with no significant weight loss, indicating no or minor distress or suffering due to treatments (Figure 2F).

Analysis of the expression of molecular targets of palbociclib and miR-199a-3p in TG221-derived HCC samples yielded results similar to what was observed *in vitro* (Figure S8). The combination of the two agents produced a decrease in both phosphorylated RB1 (S780) as well as phosphorylated AKT (S473) proteins. The downregulation of PAK4, an miR-199a-3p direct target, confirmed miRNA mimics activity in tumor cells. These findings justify the synergistic anti-tumor effect observed in the combination experimental arm. Furthermore, to explore possible additional mechanisms involved in anti-tumor effects, we performed transcriptome RNA-sequencing analyses on TG221-derived HCC treated with either single agents or the combination. A gene set enrichment analysis (GSEA) revealed that multiple gene sets involved in cell cycle, cellular response to stimuli or stress and DNA repair hallmarks were significantly depleted in mice treated with miR-199a-3p and palbociclib combination versus CTRL group (Table S2).

miR-199a-3p enhances palbociclib efficacy on sorafenib-resistant HCC cells

As the efficacy of sorafenib is hampered by the emergence of resistance to treatment, we investigated whether the combination of palbociclib and miR-199a-3p could represent a useful approach to overcome resistance to sorafenib. Here, we provided a proof of principle.

First, to develop HCC cells resistant to sorafenib, the H55.1C mouse cells were injected subcutaneously into the lateral backside of C57BL/6 female mice. After tumor appearance, mice were treated with sorafenib (30 mg/kg) (Figure S9A). Tumor xenografts were sensitive to sorafenib during the first month of treatment. Afterward some began to regrow and became insensitive to sorafenib (Figure S9B). To confirm that these cells were indeed resistant to sorafenib, xenograft-derived cells were isolated and re-implanted into the flanks of C57BL/6 mice; after tumor appearance, four mice were treated with sorafenib and the remaining four were left untreated (Figure S9C). We observed no significant difference in tumor growth between mice treated with sorafenib in comparison with untreated controls, thus confirming that these cells were stably resistant to sorafenib (Figure S9D). As we previously did with human cell lines, we evaluated basal levels of RB1 and p-RB1 protein in both H55.1C and H55.1 sorafenib-resistant cells (Figure S10).

Then, to assess whether the combination of palbociclib and miR-199a-3p could overcome resistance to sorafenib, we first demonstrated that an enforced expression of miR-199a-3p improved palbociclib efficacy on mouse sorafenib-resistant HCC cells growth *in vitro* (Figures S11A and S11B). Next, we investigated the effect *in vivo*. To this aim, since subcutaneous tumors can hardly be reached by systemic delivery of miRNA mimics (data not shown), H55.1C sorafenib-resistant cells were transduced with either AAVV-199 or AAVV-CTRL (MOI = 500). Cells were then subcutaneously implanted into the right or the left side, respectively, of C57BL/6 female mice. After tumor appearance, mice were randomly split into the following groups: (1) no treatment; (2) palbociclib (100 mg/kg); (3) sorafenib (30 mg/kg) (Figure 3A). Palbociclib efficacy was enhanced by the enforced expression of miR-199a-3p. Tumor xenografts from AAVV-199 transduced cells revealed a significantly better control on tumor growth in comparison with tumors originating from cells transduced with AAVV-CTRL (Figures 3B–3E), thus indicating a cooperative effect of the palbociclib + miR-199a-3p (confirmed by miRNA high expression at the end of experiment) combination in sorafenib-resistant cells too (Figures 3F and 3G).

Combined palbociclib/miR-199a-3p is an effective and better tolerated therapy after sorafenib

An important limitation to the use of sorafenib in patients with advanced HCC is drug tolerability.[31] Here, we investigated whether the administration of palbociclib and miR-199a-3p combination following sorafenib treatment could be better tolerated while maintaining a therapeutic efficacy in TG221 mice.

At 6 months of age, all TG221 DEN-treated mice (male mice treated with the carcinogen N-diethylnitrosoamine) exhibited multiple tumor nodules in their livers. At that time, sorafenib was administered as first-line treatment (two cycles of 21 days) to all mice. Then, mice were subdivided into three experimental groups: (1) no treatment; (2) sorafenib continuation (30 mg/kg); and (3) palbociclib (100 mg/kg) + miR-199a-3p mimics (5 mg/kg) combination. These latter approaches lasted for 21 days (Figure 4A). Sizes of tumor nodules were monitored by ultrasound analysis, and mean tumor size for the different treated groups was reported (Table S3). During the first two rounds of sorafenib (42 days), liver tumor nodules were all responsive to therapy, as shown by the reduction or stability of sizes of tumor nodules. During the following 21 days, sorafenib removal

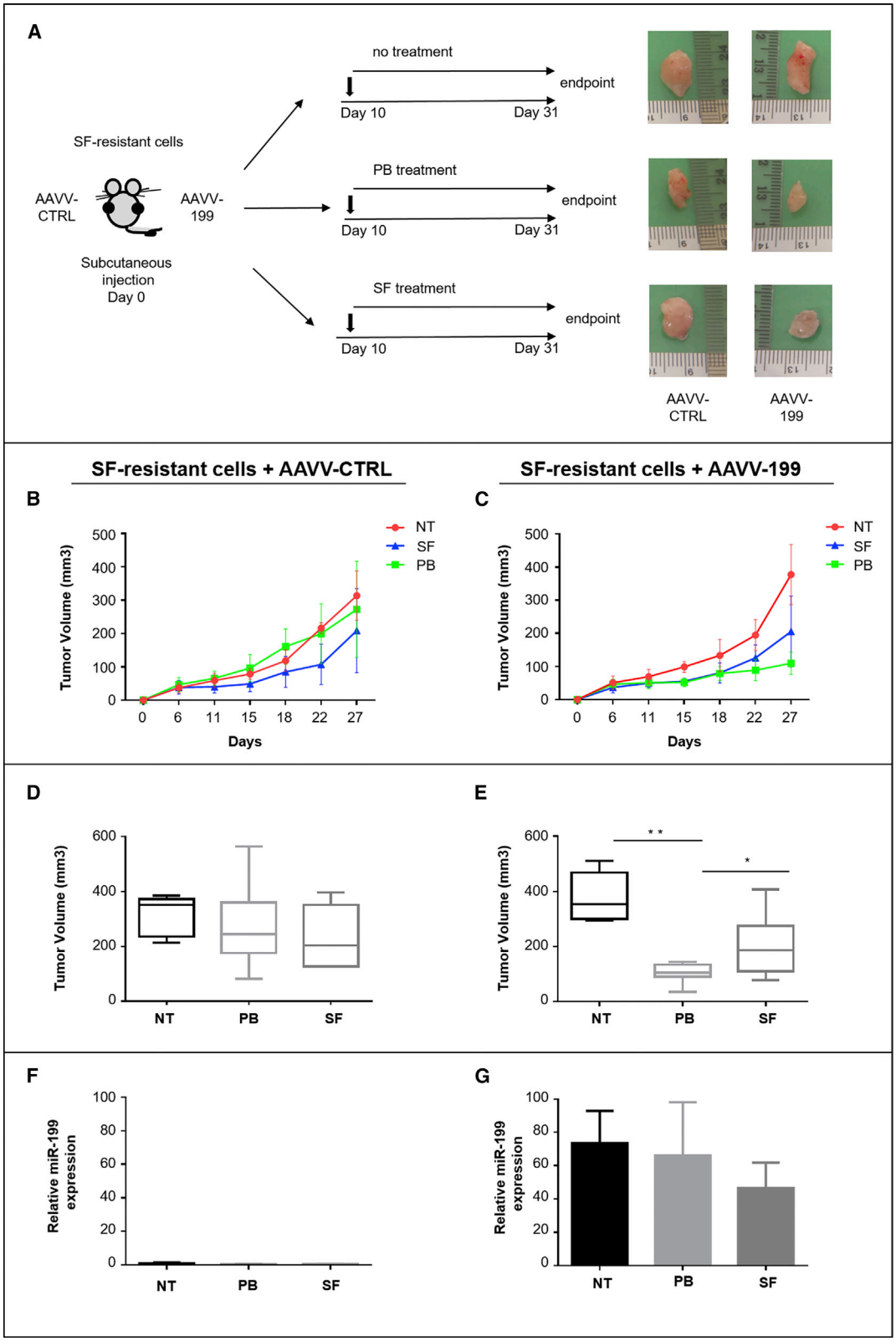

(legend on next page)

led tumors to grow back (Figure 4B); sorafenib continuation exhibited a very effective anti-tumor activity (Figure 4C), but could be hardly tolerated, as shown by the significant weight loss shown by all mice (Figure 4F); combination of palbociclib and miR-199a-3p exhibited both a good therapeutic efficacy (Figure 4D) and a good tolerability, as no weight loss was observed (Figure 4G).

DISCUSSION

Anti-cancer miRNA-based therapies are spawning a growing research interest. Restoration of tumor suppressor miRNAs or inhibition of oncogenic miRNAs are approaches that have been tested in a number of pre-clinical models, including liver cancer. Furthermore, a few clinical trials based on miRNA modulation as a strategy for cancer treatment are presently ongoing (ClinicalTrials.gov Identifier: NCT01829971; NCT02369198; NCT02580552; NCT03713320).[32-34]

In this study, we hypothesized that, rather than single agents, miRNA-based therapies could possibly be more effective if used in combination with drugs already in clinical use either to increase their efficacy or reduce their toxic effects or contrast the appearance of resistance phenomena. In this study we investigated miR-199a-3p in combination with palbociclib in *in vitro* and *in vivo* HCC experimental models. Some of the above-mentioned hypotheses were proven by results of this study.

We have previously shown that *in vivo* administration of miR-199a-3p exhibits an anti-tumor activity in TG221 mice and is well tolerated by mice.[15,16,35] The tumor-suppressing activity of miR-199a-3p has been also reported in subcutaneous, orthotopic HCC tumor models[19-21] and in patient-derived HCC xenograft (PDX) models.[22] As mechanism of action, miR-199a-3p enforced expression was shown to modulate MTOR and PAK4 oncoproteins, both essential factors of the PI3K-AKT-PTEN molecular pathway involved in cell survival and proliferation.[17,18]

Palbociclib is currently being tested in patients who failed or are intolerant to standard first-line therapy with sorafenib[7] (NCT01356628). The use of palbociclib in combination with other drugs in HCC models has also been tested. Digiacomo et al. provided evidence for the effectiveness of palbociclib and regorafenib combination in HCC cell models, where the drug combination inhibited cell proliferation and induced cell death more strongly than individual drugs.[36] Combination of palbociclib with sorafenib showed additive effects in human HCC xenografts models.[37]

Here, we tested miR-199a-3p for its ability to enhance anti-cancer activity of palbociclib in the TG221 mouse model. We previously demonstrated that this miR-221 transgenic mouse model represents a fairly accurate valuable model of liver cancer to perform pre-clinical investigations aimed at testing miRNA-based therapies. In addition to the up-regulation of miR-221, other miRNAs known to play a key role in human HCC, such as miR-199a-3p, or miR-122 or miR-21 were dysregulated in tumors arising in the TG221 model similarly to human HCC.[35]

The rationale for the use of palbociclib in combination with miR-199a-3p is based on the fact that palbociclib, while suppressing CDK4/6 kinase activity, at the same time increases AKT activity. Hence, we hypothesize that inhibition of the AKT pathway could synergize with palbociclib to enhance anti-cancer activity. Indeed, we confirmed the value of the hypothesis by detecting a strong synergistic effect between palbociclib and the pan-AKT inhibitor, MK-2206. However, heavy toxicity hampered the possibility of using this combination *in vivo*. Conversely, the combination of miR-199a-3p with palbociclib demonstrated a good therapeutic efficacy and an excellent tolerability, providing a pre-clinical proof of principle of the value of miR-199a-3p and palbociclib combination in anti-HCC therapy. These results suggest inhibition of AKT activity represents a general approach to increase anti-tumor palbociclib efficacy.

The basis for using CDK4/6 inhibitors, like palbociclib, as anti-cancer agents is the presence of RB1-proficient cells, as RB1 protein is a major target phosphorylated by CDK4/6. However, the observed palbociclib-induced downregulation of RB1 protein is puzzling as it would go against the tumor suppressor function of RB1. While we have no explanation for the finding, as molecular mechanisms leading to RB1 protein decrease is presently unknown, our results are in agreement with other reports that have previously shown that palbociclib causes a decrease in levels of total RB1 protein together with a decrease of its phosphorylation.[36]

Moreover, our results are in contrast with the idea that inhibition of RB1 phosphorylation is the sole mechanism associated with palbociclib anti-tumor action, considering that its growth inhibitory effect is also observed in Hep3B cells, which carry an STOP codon in the *RB1* gene and present an intrinsic very low expression of RB1 protein. Instead, this study highlights the importance of *FOXM1*, an oncogenic transcription factor master regulator of cell cycle progression[38] aberrantly expressed in several human cancers, including HCC,[39] which is a substrate of CDK4/6.[40] FOXM1 exhibits a similar and potentially even more relevant state, as it presents oncogenic activity. In fact, its lack of phosphorylation by CDK4/6 promotes its degradation and inhibition of its activity. Furthermore, inhibition of FOXM1, which is also activated via the AKT pathway,[29,30] can be at the same time sustained by miR-199a-3p.

Figure 3. miR-199a-3p enhanced palbociclib therapeutic effect on xenografts of sorafenib-resistant cells

(A) AAVV-199 transduced SF-resistant cells were implanted into the right side, while AAVV-CTRL transduced cells were implanted into the left side of each mouse. (B and C) When tumor reached a volume of ~50 mm^3 (10 days after injection of cells), mice received the following treatments: (1) not treated (NT) (n = 5); (2) palbociclib (PB) (n = 10); (3) sorafenib (SF) (n = 10). Size of tumor nodules was measured with a caliper every 2 days until euthanization. (D and E) Endpoint mean tumor volume; (F and G) miR-199a-3p expression levels in tumors at time of euthanization. Data are represented as mean ± SD. *p value $\leq$0.05; **p value $\leq$0.01.

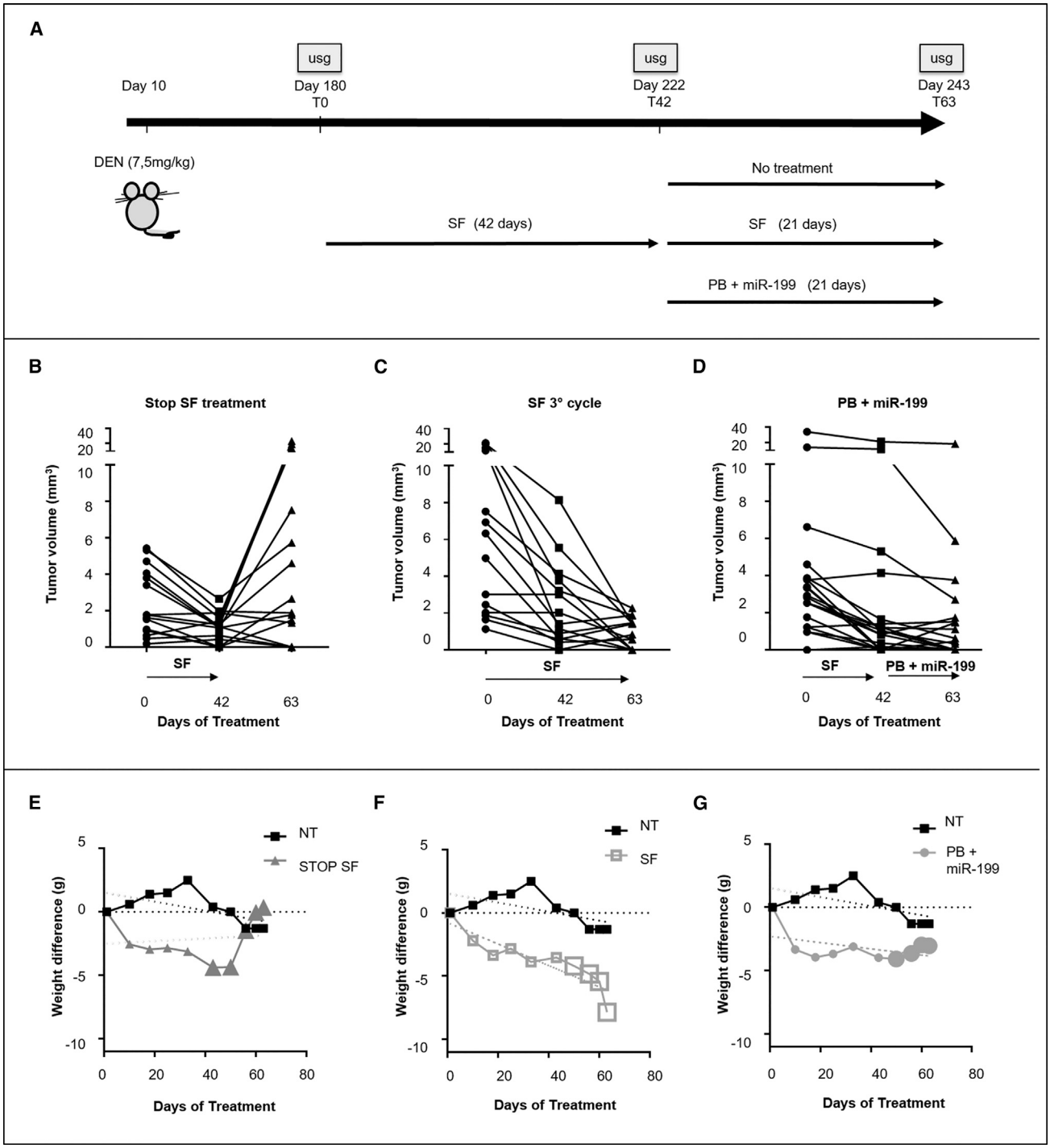

Figure 4. Palbociclib in combination with miR-199a-3p represents an effective and better tolerated therapy after sorafenib treatment

(A) At 6 months of age, all DEN-treated mice were treated with sorafenib (two cycles of 21 days each) as a first-line treatment. Then, mice were split into three groups and treated for an additional 21 days as follows: (1) no further treatment (n = 3); (2) sorafenib (SF) (n = 3); (3) combination of palbociclib + miR-199a-3p mimics (PB + miR199) (n = 3). Tumor growth was monitored with ultrasound (usg) at the beginning and at the end of each treatment. Results indicated that the suspension of sorafenib treatment led to a reduction of toxicity effects (E) but also tumors grew back (B). Continuation of sorafenib led to a reduction of tumor growth (C) but also to a critical weight loss. (D) PB + miR-199 combination led to a reduction of tumor nodule sizes and was well tolerated (G).

As a more general indication, this study suggests that miRNA-based therapy could find a useful application through the combination with drugs already in use in the clinic to improve their effectiveness without increasing toxicity. In fact, an important limitation to the use of sorafenib is its toxic side effects during long-term treatments.[41] This toxic effect was confirmed in TG221 mice: we showed that a continuous administration of sorafenib (three cycles of 21 days each) was effective in terms of anti-tumor efficacy, but poorly tolerated by treated mice, as shown by a dangerous body weight loss. Replacement of sorafenib in the third cycle with palbociclib + miR-199a-3p combination could overcome this problem, it offered a therapeutic strategy that was effective both in terms of efficacy against tumor growth and in term of tolerability. Finally, our results demonstrated that administration of palbociclib together with miR-199a-3p can reduce the growth of sorafenib-resistant xenograft tumors, providing evidence of the potential efficacy of these drugs as a new therapeutic option to contrast the emergence of sorafenib resistance. While any anti-cancer treatment is prone to fail because of development of acquired resistance, a combination of drugs is expected to reduce the risk of resistance but is generally flawed by an increased toxicity. This was indeed the case of the combination of palbociclib and MK-2206 described in this study. However, by replacing the AKT inhibitor with an miRNA-based approach, we proved that the combination of palbociclib with miR-199a-3p could represent an effective option against sorafenib-resistant cells without increasing toxicity. Long-term experiments will be needed to assess how long the effect may last, before other mechanisms of resistance develop.

In summary, our findings suggest an miRNA-based alternative to sorafenib that can potentially be considered in addition to available therapies in advanced HCC. It also suggests a general strategy for the use of miRNA-based molecules to improve the anti-tumor efficacy of drugs without producing adverse toxicities, thus providing this additional value to their potential use in a clinical setting. This study establishes a proof of principle for carrying out further pre-clinical investigations, such as evaluation of the effect of the combined treatment on PDX models generated from sorafenib sensitive, sorafenib-resistant, or metastatic human tumors, aimed at establishing the ground for future clinical trials.

MATERIALS AND METHODS

Cell culture

The HCC cell lines Hep3B (HB-8064) and HepG2 (HB-8065) were obtained from the American Type Culture Collection (ATCC, Manassas, VA, USA). The human embryonic kidney cells 293FT were obtained from Invitrogen (Carlsbad, CA, USA). H55.1C mouse cells, established from a primary hepatoma of C57BL/6J mice, were obtained from CLS Cell Lines Service GmbH, Germany. Cell lines were propagated and maintained in Dulbecco's modified Iscove's Medium (IMDM) supplemented with 10% fetal bovine serum (FBS), 0.1% gentamycin, and 1% L-glutamine (Sigma-Aldrich, St. Louis, MO, USA). All cell lines were authenticated by the provider and tested free of mycoplasma contamination (MycoAlert Mycoplasma Detection kit, LT07-418, Lonza Group Ltd, Basel, Switzerland). *In vitro* cell transfections were performed using Lipofectamine 2000 (Invitrogen).

Cell viability and apoptosis assays

The Muse Count & Viability Kit was used to perform quantitative analysis of cell count and viability (MCH100102, Luminex Corporation, Austin, TX, USA). The Muse Annexin V and Dead Cell Assay kit (MCH100105, Luminex Corporation) was used to measure viable, apoptotic, and dead cells. All assays were performed in triplicate and analyzed in a Muse Cell Analyzer instrument (Merck Millipore).

Anti-tumor drugs

For *in vitro* experiments, all drugs were solubilized in dimethyl sulfoxide (DMSO). For all *in vivo* experiments, drugs were administered daily by oral gavage as indicated by the manufacturer's instructions: sorafenib (S-8599, LC Laboratories, Woburn, MA, USA) was dissolved in a 50:50 Cremophor EL and ethanol solution; MK2206 (MK2206 dihydrochloride, Medchem Express, HY-10358-0002, NJ, USA) was dissolved in 15% Captisol (SBE-b-CD, Medchem Express, HY-17031-0731); palbociclib (palbociclib Isethionate Salt, CAS No. 827,022-33-3, BOC sciences, Shirley, NY, USA) was dissolved in sodium lactate buffer (50 mM, pH 4.0)

Recombinant AAVVs

The AAVV expressing miR-199a-3p (AAVV-199) and the AAVV-CTRL vector, expressing the GFP, were previously described.[15]

RNA mimics for *in vivo* therapies

miR-199a-3p mimics and *scrambled* unmodified single-stranded RNA oligonucleotides were obtained from Axolabs GmbH (Kulmbach, Germany). The oligonucleotide sequences were as follows: (1) miR-199a-3p mimic sequence 5′-ACAGUAGUCUGCACAUUG GUUA-3′ (unmodified sequence); (2) *scramble* sequence 5′-UCA-CAACCUCCUAGAAAGAGUAGA-3′ (unmodified sequence). For *in vivo* delivery, lipid nanoparticles were used as vehicle.

Lipid nanoparticles

The lipid components of the nanoparticles were 1,2-dioleoyl-sn-glycero-3-phosphoethanolamine (DOPE), 1,2-dimyristoyl-sn-glycerol, methoxypolyethylene glycol (DMG-PEG, Mw 2,000; #15091, Cayman Chemical Company, Ann Arbor, MI, USA), and linoleic acid (#L1376, Sigma-Aldrich, St. Louis, MO, USA). The preparation of empty nanoparticles was performed as previously described.[42]

In vivo mouse studies

The study was performed according with the Guidelines for the Care and Use of Laboratory Animals of the Italian Ministry of Health. All animals received human care and ensured that study protocols comply with the institution's guidelines. All studies involving animal experiments are compliant with the Animal Research: Reporting of In Vivo Experiments (ARRIVE) guidelines. To comply with the 2010/63/EU directive of the European Parliament and Council, enforced by the Italian law requiring a minimized number of experimental animals, G*Power (http://www.gpower.hhu.de/) was used to

define the sample size for the experiments. All animals were randomly assigned to different treatment groups at the start of the studies. The protocols for animal experimentation were approved by the Italian Ministry of Health (approval no. 701/2017-PR and no. 645/2021-PR).

The TG221 transgenic mouse used in the experiments, characterized by the overexpression of miR-221 in the liver and predisposed to the development of liver tumors. was already described.[35] C57BL/6J wild-type female mice (6–8 weeks old) were obtained from Charles River Laboratories s.r.l., Calco, Italy. All mice were maintained in vented cabinets at 25°C with 12-h light-dark cycle, with food and water *ad libitum*.

TG221 experiments: to facilitate tumor development, 10-day newborn male mice received one i.p. injection of DEN (#N0756, Sigma-Aldrich) (7.5 mg/kg body weight). Mice were monitored for the presence of hepatic lesions using an ultrasound diagnostic device (Philips IU22) as previously described.[16] Mice were randomly enrolled for treatments at 6 months of age.

Xenograft experiments: (1) To obtain sorafenib-resistant xenograft tumors, mice were injected subcutaneously into the lateral backside with 5×10^4 H55.1C mouse cells diluted 1:1 in Matrigel (Matrigel Basement Membrane Matrix, High Concentration, phenol red-free, #354262; Corning, NY, USA). When tumor reached a volume of ~50 mm^3 (10 days after cell injection), mice were randomly enrolled for treatments. Tumor lengths (major tumor axis) and widths (minor tumor axis) were measured at a regular interval of 2 days from their first appearance and tumor volumes were calculated according to the formula: Tum Vol = $width^2 \times length \times 0.5$. At the end of the treatment, mice were euthanized and tumor xenografts resistant to sorafenib were collected. To obtain *in vivo* selected sorafenib-resistant cells (SF-resistant cells), small slices of tumor xenograft tissues were cultured in complete IMDM Medium in presence of sorafenib. (2) To test the therapeutic effect of miR-199a-3p in combination with palbociclib, SF-resistant cells were first transduced *in vitro* with AAVV-199 (MOI = 500) or with AAVV-CTRL (MOI = 500) as a control. After 24 h, 5×10^4 cells were then subcutaneously implanted into the right or the left side, respectively, of C57BL/6 female mice as described above. When tumor reached a volume of ~50 mm^3 (10 days after cell injection), mice were randomly enrolled for treatments. At the end of the all *in vivo* experiments, mice were euthanized, tumor tissues were collected, immediately frozen in liquid nitrogen, and stored at −80°C or fixed in 10% phosphate-buffered formalin for 12 to 24 h and embedded in paraffin for histological analysis.

Western blot analyses

Cell cultures were collected at the indicated time point and then washed with PBS. Tissue samples were collected, immediately frozen in liquid nitrogen, and stored at −80°C until protein extraction. All samples were dissolved in radioimmune precipitation (RIPA) Buffer (#R0278; Sigma-Aldrich) containing phosphatase and protease inhibitors (#P2850 and #P8340; Sigma-Aldrich). Lysates were centrifuged at 8,000 × *g* for 10 min at 4°C to pellet the debris, and supernatants were collected. Protein concentrations were measured with Bradford assay (#500-0205, Bio-Rad, Hercules, CA, USA). Equal amounts (30 μg) of protein extracts from all samples were applied to SDS–PAGE electrophoresis (4%–15% Tris Glycine Gel, #4561083, Bio-Rad) and then transferred to a PVDF membrane (#1704156, Bio-Rad). After incubation with 5% Blocking agent, the membrane were incubated overnight at 4°C with the following antibodies and specific conditions: Rabbit antibodies against p-RB (Ser780, D59B7, #8180), p-AKT (Ser473, D9E XP, #4060), p-FOXM1 (Thr600, D9M6G, #14655), RB (D20, #9313), FOXM1 (D12D5, #5436) and PAK4 (#3242) were all from Cell Signaling Technology (Danvers, MA, USA) and were diluted in 5% w/v BSA (A4503, Sigma-Aldrich), 1X Tris-buffered saline (TBS; Bio-Rad Laboratories, Hercules, CA, USA), and 0.1% Tween 20 (Bio-Rad) and incubated at 4°C for 16 h. Rabbit antibody against AKT (C-20, sc-1618) was obtained from Santa Cruz Biotechnology (Dallas, TX, USA) and was diluted in 1% w/v milk, 1X TBS, and 0.1% Tween 20 (Bio-Rad). The anti-glyceraldehyde-3-phosphate dehydrogenase (GAPDH) monoclonal antibody (clone 2D9, TA802519; OriGene Technologies, Rockville, MD, USA) was used as a loading control. For chemiluminescent detection, a horseradish peroxidase (HRP)-conjugated secondary antibody (#7074; Cell Signaling Technology) was used in combination with Clarity Western ECL Blotting Substrate (#170-5060; Bio-Rad) and digital images were acquired using a Chemidoc (Bio-Rad). Signals were quantified with ImageJ software (https://imagej.nih.gov) and protein expression levels were normalized according to the expression of the housekeeping protein.

Histological and immunohistochemistry procedures

Tissue samples from at least two representative fragments of each lobe of the liver were taken at autopsy and fixed in 10% phosphate-buffered formalin for 12 to 24 h and embedded in paraffin. Serial sections were stained with H&E for the histological determination of nodules dimensions and for the assessment of tumor-infiltrating lymphocytes. The presence and localization of Cleaved Caspase 3 and Ki67 proteins in liver tissues from transgenic mice were immunohistochemically assessed on formalin-fixed, paraffin-embedded sections. Serial 4-μm-thick sections were processed. Cleaved Caspase-3 (Asp175) (D3E9) Rabbit mAb (#9579, Cell Signaling) and Ki-67 (D2H10) Rabbit mAb (#9027, Cell Signaling) were diluted in SignalStain Antibody Diluent (#8112, Cell Signaling) and detected by the polymer-based, HRP-conjugated SignalStain Boost IHC Detection Reagent (#8114) in combination with SignalStain DAB Diluent (#11724, Cell Signaling) and Chromogen Concentrate (#11725, Cell Signaling), following the manufacturer instructions. To verify the specificity of staining, a concentration-matched rabbit monoclonal immunoglobulin G control was used. After rinsing in distilled water, slides were counterstained with Leica Microsystem's hematoxylin (Fisher Scientific, Italy) and mounted with Micromount mounting media (Diapath, Italy, SKU060500). For apoptosis and proliferation evaluation, six separate areas of cleaved caspase-3- and Ki-67-stained tissues were analyzed. The percentage of cleaved caspase-3 or Ki-67-positive stained area was calculated per selected region and the results were quantified by ImageJ software.

Reverse transcription and droplet digital polymerase chain reaction

Total RNA was extracted from cells or from frozen liver tissues using the automated Maxwell Rapid Sample Concentrator Instrument (Promega Corporation, Madison, WI, USA) with the purification kit Maxwell RSC miRNA from Tissue (#AS1460, Promega) according to the manufacturer's instructions. Droplet digital polymerase chain reaction (ddPCR) was used to measure the expression level of miRNAs. For quantitative PCR analysis, 5 ng of purified RNA were retro-transcribed using TaqMan MicroRNA Reverse Transcription kit (Applied Biosystems, Foster City, CA, USA) and cDNA was used for amplification as previously described.[15] A TaqMan miRNA PCR probe set specific for miR-199a-3p (assay ID002304; Applied Biosystems) was used, while a TaqMan Assays for RNAs U6 (assay ID001973; Applied Biosystems) was used to normalize the relative abundance of miRNAs.

RNA sequencing

After RNA quality and integrity check by Bioanalyzer 2100 and Agilent RNA 6000 Nano Kit (# 5067-1511 Agilent, Santa Clara, CA, USA), RNA-sequencing libraries were prepared using Qiagen QIAseq Fast Select rRNA HMR kit (#334386, Qiagen Düsseldorf, Germany) for ribosomal RNA depletion and Qiagen QIAseq stranded total RNA library kit (#180745, Qiagen) according to the manufacturer's instructions. RNA sequencing was carried out according to the Illumina pipeline on a NextSeq 500 Instrument (Illumina, San Diego, CA, USA.) using NextSeq 500/550 High Output Kit v2.5 150 Cycles (#20024907, Illumina).

Bioinformatics analysis

Obtained sequences were mapped to the human genome (GRCm38) using the algorithm HISAT2 [https://pubmed.ncbi.nlm.nih.gov/25751142/] and a pre-built genome index downloadable form HISAT2 website. Then, StringTie [https://pubmed.ncbi.nlm.nih.gov/25690850/] was used to assemble and quantify the transcripts in each sample. Finally, expressed transcripts have been normalized using the DeSeq2 [https://pubmed.ncbi.nlm.nih.gov/25516281/] package for R. GSEA [https://pubmed.ncbi.nlm.nih.gov/16199517/] was performed using GSEA 4.1.0 with a database containing hallmark gene sets from MSigDB collection and canonical pathways gene sets derived from the Reactome pathway database. Significant gene sets were selected to have a false discovery rate adjusted p value < 0.05.

Statistical analysis

To assess the statistical significance of group similarity, we used the t test when the variance of the two compared samples were equal, or Welch's t test when two samples exhibited unequal variances. Test was considered statistically significant at p value $\leq$ 0.05. Variances between groups were assessed by the F-test. When appropriate, data values were expressed in terms of mean ± SD. GraphPad Prism 6.0 (GraphPad Software, La Jolla, CA, USA) was used for data analysis. No samples or animals were excluded from the analyses.

DATA AVAILABILITY

The authors declare that all data supporting the findings of this study are available within the article and its Supplemental information files.

SUPPLEMENTAL INFORMATION

Supplemental information can be found online at https://doi.org/10.1016/j.omtn.2022.07.015.

ACKNOWLEDGMENTS

This work was supported by funding from the Italian Association for Cancer Research (AIRC IG-20055) and by funds from the University of Ferrara to M.N., S.S., and E.C.

AUTHOR CONTRIBUTIONS

E.C., S.S., and M.N. conceived and designed research; E.C., P.G., C.B., L.D.A., and E.S. performed all the experiments and the acquisition, analysis, and interpretation of data; E.C., S.S., and M.N. wrote the manuscript; A.F., A.L., and E.M.S. contributed to a critical revision of the manuscript; all the authors read and approved the manuscript.

DECLARATION OF INTERESTS

The authors declare no competing interests.

REFERENCES

1. Bray, F., Ferlay, J., Soerjomataram, I., Siegel, R.L., Torre, L.A., and Jemal, A. (2018). Global cancer statistics 2018: GLOBOCAN estimates of incidence and mortality worldwide for 36 cancers in 185 countries. CA. Cancer J. Clin. *68*, 394–424.
2. Gordan, J.D., Kennedy, E.B., Abou-Alfa, G.K., Beg, M.S., Brower, S.T., Gade, T.P., Goff, L., Gupta, S., Guy, J., Harris, W.P., et al. (2020). Systemic therapy for advanced hepatocellular carcinoma: ASCO guideline. J. Clin. Oncol. *38*, 4317–4345.
3. Llovet, J.M., Kelley, R.K., Villanueva, A., Singal, A.G., Pikarsky, E., Roayaie, S., Lencioni, R., Koike, K., Zucman-Rossi, J., and Finn, R.S. (2021). Hepatocellular carcinoma. Nat. Rev. Dis. Primers *7*, 6.
4. De Mattia, E., Cecchin, E., Guardascione, M., Foltran, L., Di Raimo, T., Angelini, F., D'Andrea, M., and Toffoli, G. (2019). Pharmacogenetics of the systemic treatment in advanced hepatocellular carcinoma. World J. Gastroenterol. *25*, 3870–3896.
5. Beaver, J.A., Amiri-Kordestani, L., Charlab, R., Chen, W., Palmby, T., Tilley, A., Zirkelbach, J.F., Yu, J., Liu, Q., Zhao, L., et al. (2015). FDA approval: palbociclib for the treatment of postmenopausal patients with estrogen receptor-positive, HER2-negative metastatic breast cancer. Clin. Cancer Res. *21*, 4760–4766.
6. Walker, A.J., Wedam, S., Amiri-Kordestani, L., Bloomquist, E., Tang, S., Sridhara, R., Chen, W., Palmby, T.R., Fourie Zirkelbach, J., Fu, W., et al. (2016). FDA approval of palbociclib in combination with fulvestrant for the treatment of hormone receptor-positive, HER2-negative metastatic breast cancer. Clin. Cancer Res. *22*, 4968–4972.
7. Littman, S.J., Brus, C., and Burkart, A. (2015). A phase II study of palbociclib (PD-0332991) in adult patients with advanced hepatocellular carcinoma. J. Clin. Oncol. *33*, 277.
8. Fry, D.W., Harvey, P.J., Keller, P.R., Elliott, W.L., Meade, M., Trachet, E., Albassam, M., Zheng, X., Leopold, W.R., Pryer, N.K., and Toogood, P.L. (2004). Specific inhibition of cyclin-dependent kinase 4/6 by PD 0332991 and associated antitumor activity in human tumor xenografts. Mol. Cancer Ther. *3*, 1427–1438.
9. Rubio, C., Martínez-Fernández, M., Segovia, C., Lodewijk, I., Suarez-Cabrera, C., Segrelles, C., López-Calderón, F., Munera-Maravilla, E., Santos, M., Bernardini, A., et al. (2019). CDK4/6 inhibitor as a novel therapeutic approach for advanced bladder cancer independently of RB1 status. Clin. Cancer Res. *25*, 390–402.
10. Zhang, J., Xu, K., Liu, P., Geng, Y., Wang, B., Gan, W., Guo, J., Wu, F., Chin, Y.R., Berrios, C., et al. (2016). Inhibition of Rb phosphorylation leads to mTORC2-mediated activation of akt. Mol. Cell *62*, 929–942.

11. Cretella, D., Ravelli, A., Fumarola, C., La Monica, S., Digiacomo, G., Cavazzoni, A., Alfieri, R., Biondi, A., Generali, D., Bonelli, M., and Petronini, P.G. (2018). The anti-tumor efficacy of CDK4/6 inhibition is enhanced by the combination with PI3K/AKT/mTOR inhibitors through impairment of glucose metabolism in TNBC cells. J. Exp. Clin. Cancer Res. *37*, 72.

12. Bonelli, M.A., Digiacomo, G., Fumarola, C., Alfieri, R., Quaini, F., Falco, A., Madeddu, D., La Monica, S., Cretella, D., Ravelli, A., et al. (2017). Combined inhibition of CDK4/6 and PI3K/AKT/mTOR pathways induces a synergistic anti-tumor effect in malignant pleural mesothelioma cells. Neoplasia *19*, 637–648.

13. Simioni, C., Neri, L.M., Tabellini, G., Ricci, F., Bressanin, D., Chiarini, F., Evangelisti, C., Cani, A., Tazzari, P.L., Melchionda, F., et al. (2012). Cytotoxic activity of the novel Akt inhibitor, MK-2206, in T-cell acute lymphoblastic leukemia. Leukemia *26*, 2336–2342.

14. Yap, T.A., Yan, L., Patnaik, A., Fearen, I., Olmos, D., Papadopoulos, K., Baird, R.D., Delgado, L., Taylor, A., Lupinacci, L., et al. (2011). First-in-man clinical trial of the oral pan-AKT inhibitor MK-2206 in patients with advanced solid tumors. J. Clin. Oncol. *29*, 4688–4695.

15. Callegari, E., D'Abundo, L., Guerriero, P., Simioni, C., Elamin, B.K., Russo, M., Cani, A., Bassi, C., Zagatti, B., Giacomelli, L., et al. (2018). miR-199a-3p modulates MTOR and PAK4 pathways and inhibits tumor growth in a hepatocellular carcinoma transgenic mouse model. Mol. Ther. Nucleic Acids *11*, 485–493.

16. Callegari, E., Domenicali, M., Shankaraiah, R.C., D'Abundo, L., Guerriero, P., Giannone, F., Baldassarre, M., Bassi, C., Elamin, B.K., Zagatti, B., et al. (2019). MicroRNA-based prophylaxis in a mouse model of cirrhosis and liver cancer. Mol. Ther. Nucleic Acids *14*, 239–250.

17. Engelman, J.A. (2009). Targeting PI3K signalling in cancer: opportunities, challenges and limitations. Nat. Rev. Cancer *9*, 550–562.

18. Tyagi, N., Bhardwaj, A., Singh, A.P., McClellan, S., Carter, J.E., and Singh, S. (2014). p-21 activated kinase 4 promotes proliferation and survival of pancreatic cancer cells through AKT- and ERK-dependent activation of NF-kappaB pathway. Oncotarget *5*, 8778–8789.

19. Hou, J., Lin, L., Zhou, W., Wang, Z., Ding, G., Dong, Q., Qin, L., Wu, X., Zheng, Y., Yang, Y., et al. (2011). Identification of miRNomes in human liver and hepatocellular carcinoma reveals miR-199a/b-3p as therapeutic target for hepatocellular carcinoma. Cancer Cell *19*, 232–243.

20. Ghosh, A., Dasgupta, D., Ghosh, A., Roychoudhury, S., Kumar, D., Gorain, M., Butti, R., Datta, S., Agarwal, S., Gupta, S., et al. (2017). MiRNA199a-3p suppresses tumor growth, migration, invasion and angiogenesis in hepatocellular carcinoma by targeting VEGFA, VEGFR1, VEGFR2, HGF and MMP2. Cell Death Dis. *8*, e2706.

21. Varshney, A., Panda, J.J., Singh, A.K., Yadav, N., Bihari, C., Biswas, S., Sarin, S.K., and Chauhan, V.S. (2018). Targeted delivery of miR-199a-3p using self-assembled dipeptide nanoparticles efficiently reduces hepatocellular carcinoma. Hepatology *67*, 1392–1407.

22. Shao, S., Hu, Q., Wu, W., Wang, M., Huang, J., Zhao, X., Tang, G., and Liang, T. (2020). Tumor-triggered personalized microRNA cocktail therapy for hepatocellular carcinoma. Biomater. Sci. *8*, 6579–6591.

23. Ren, K., Li, T., Zhang, W., Ren, J., Li, Z., and Wu, G. (2016). miR-199a-3p inhibits cell proliferation and induces apoptosis by targeting YAP1, suppressing Jagged1-Notch signaling in human hepatocellular carcinoma. J. Biomed. Sci. *23*, 79.

24. Kim, J.H., Badawi, M., Park, J.K., Jiang, J., Mo, X., Roberts, L.R., and Schmittgen, T.D. (2016). Anti-invasion and anti-migration effects of miR-199a-3p in hepatocellular carcinoma are due in part to targeting CD151. Int. J. Oncol. *49*, 2037–2045.

25. Fornari, F., Milazzo, M., Chieco, P., Negrini, M., Calin, G.A., Grazi, G.L., Pollutri, D., Croce, C.M., Bolondi, L., and Gramantieri, L. (2010). MiR-199a-3p regulates mTOR and c-Met to influence the doxorubicin sensitivity of human hepatocarcinoma cells. Cancer Res. *70*, 5184–5193.

26. Henry, J.C., Park, J.K., Jiang, J., Kim, J.H., Nagorney, D.M., Roberts, L.R., Banerjee, S., and Schmittgen, T.D. (2010). miR-199a-3p targets CD44 and reduces proliferation of CD44 positive hepatocellular carcinoma cell lines. Biochem. Biophys. Res. Commun. *403*, 120–125.

27. Lou, G., Chen, L., Xia, C., Wang, W., Qi, J., Li, A., Zhao, L., Chen, Z., Zheng, M., and Liu, Y. (2020). MiR-199a-modified exosomes from adipose tissue-derived mesenchymal stem cells improve hepatocellular carcinoma chemosensitivity through mTOR pathway. J. Exp. Clin. Cancer Res. *39*, 4.

28. Lee, H.A., Chu, K.B., Moon, E.K., and Quan, F.S. (2021). Histone deacetylase inhibitor-induced CDKN2B and CDKN2D contribute to G2/M cell cycle arrest incurred by oxidative stress in hepatocellular carcinoma cells via forkhead box M1 suppression. J. Cancer *12*, 5086–5098.

29. Yao, S., Fan, L.Y.N., and Lam, E.W.F. (2018). The FOXO3-FOXM1 axis: a key cancer drug target and a modulator of cancer drug resistance. Semin. Cancer Biol. *50*, 77–89.

30. Chesnokov, M.S., Borhani, S., Halasi, M., Arbieva, Z., Khan, I., and Gartel, A.L. (2021). FOXM1-AKT positive regulation loop provides venetoclax resistance in AML. Front. Oncol. *11*, 696532.

31. Iyer, R., Fetterly, G., Lugade, A., and Thanavala, Y. (2010). Sorafenib: a clinical and pharmacologic review. Expert Opin. Pharmacother. *11*, 1943–1955.

32. Hong, D.S., Kang, Y.K., Borad, M., Sachdev, J., Ejadi, S., Lim, H.Y., Brenner, A.J., Park, K., Lee, J.L., Kim, T.Y., et al. (2020). Phase 1 study of MRX34, a liposomal miR-34a mimic, in patients with advanced solid tumours. Br. J. Cancer *122*, 1630–1637.

33. van Zandwijk, N., Pavlakis, N., Kao, S.C., Linton, A., Boyer, M.J., Clarke, S., Huynh, Y., Chrzanowska, A., Fulham, M.J., Bailey, D.L., et al. (2017). Safety and activity of microRNA-loaded minicells in patients with recurrent malignant pleural mesothelioma: a first-in-man, phase 1, open-label, dose-escalation study. Lancet Oncol. *18*, 1386–1396.

34. Witten, L., and Slack, F.J. (2020). miR-155 as a novel clinical target for hematological malignancies. Carcinogenesis *41*, 2–7.

35. Callegari, E., Elamin, B.K., Giannone, F., Milazzo, M., Altavilla, G., Fornari, F., Giacomelli, L., D'Abundo, L., Ferracin, M., Bassi, C., et al. (2012). Liver tumorigenicity promoted by microRNA-221 in a mouse transgenic model. Hepatology *56*, 1025–1033.

36. Digiacomo, G., Fumarola, C., La Monica, S., Bonelli, M.A., Cretella, D., Alfieri, R., Cavazzoni, A., Galetti, M., Bertolini, P., Missale, G., and Petronini, P.G. (2020). Simultaneous combination of the CDK4/6 inhibitor palbociclib with regorafenib induces enhanced anti-tumor effects in hepatocarcinoma cell lines. Front. Oncol. *10*, 563249.

37. Bollard, J., Miguela, V., Ruiz de Galarreta, M., Venkatesh, A., Bian, C.B., Roberto, M.P., Tovar, V., Sia, D., Molina-Sánchez, P., Nguyen, C.B., et al. (2017). Palbociclib (PD-0332991), a selective CDK4/6 inhibitor, restricts tumour growth in preclinical models of hepatocellular carcinoma. Gut *66*, 1286–1296.

38. Laoukili, J., Kooistra, M.R.H., Brás, A., Kauw, J., Kerkhoven, R.M., Morrison, A., Clevers, H., and Medema, R.H. (2005). FoxM1 is required for execution of the mitotic programme and chromosome stability. Nat. Cell Biol. *7*, 126–136.

39. Yu, M., Tang, Z., Meng, F., Tai, M., Zhang, J., Wang, R., Liu, C., and Wu, Q. (2016). Elevated expression of FoxM1 promotes the tumor cell proliferation in hepatocellular carcinoma. Tumour Biol. *37*, 1289–1297.

40. Anders, L., Ke, N., Hydbring, P., Choi, Y.J., Widlund, H.R., Chick, J.M., Zhai, H., Vidal, M., Gygi, S.P., Braun, P., and Sicinski, P. (2011). A systematic screen for CDK4/6 substrates links FOXM1 phosphorylation to senescence suppression in cancer cells. Cancer Cell *20*, 620–634.

41. Zhou, K., and Fountzilas, C. (2019). Outcomes and quality of life of systemic therapy in advanced hepatocellular carcinoma. Cancers *11*, E861.

42. Huang, X., Schwind, S., Yu, B., Santhanam, R., Wang, H., Hoellerbauer, P., Mims, A., Klisovic, R., Walker, A.R., Chan, K.K., et al. (2013). Targeted delivery of microRNA-29b by transferrin-conjugated anionic lipopolyplex nanoparticles: a novel therapeutic strategy in acute myeloid leukemia. Clin. Cancer Res. *19*, 2355–2367.

OMTN, Volume *29*

Supplemental information

miR-199a-3p increases the anti-tumor activity of palbociclib in liver cancer models

Elisa Callegari, Paola Guerriero, Cristian Bassi, Lucilla D'Abundo, Antonio Frassoldati, Edi Simoni, Laura Astolfi, Enrico Maria Silini, Silvia Sabbioni, and Massimo Negrini

SUPPLEMENTAL INFORMATION

SUPPLEMENTAL TABLES

Table S1. Anti-cancer activity of palbociclib, MK-2206 and their combination

	Number of mice	Tumor Volume difference between post and pre-treatment (mean ± SD, mm^3)
CTRL	13	9,80 ± 28,14
PB	6	0,55 ± 4,62
MK	6	4,63 ± 10,73
PB+MK	5	-0,01 ± 0,48

CTRL = untreated; PB= palbociclib; MK=MK-2206

Table S2. Gene Set Enrichment Analysis (GSEA) of hallmark gene sets (MSigDB collection) and canonical pathways gene sets (Reactome pathway database) in treated mice versus CTRL group

Table S3. Mean tumor size at various time points

	Tumor volume (Mean ± SD, mm^3)		
	T=0	T=42	T=63
SF (2 cycles) + STOP SF	2,44 ± 1,8	1,08 ± 0,8	5,52 ± 7,4
SF (2 cycles) + SF 3rd cycle	7,65 ±7,0	2,50 ± 2,3	0,98 ± 0,8
SF (2 cycles) + PB + miR-199	4,86 ± 7,5	2,61 ± 5,2	1,91 ± 4,2

SF=sorafenib; PB=palbociclib
Tumor volume measurement (Mean ± SD).
(T=0) day 0, before any treatment
(T=42) day 42, end of two 21-days cycles of sorafenib
(T=63) day 63, end of 3rd cycle regimen

SUPPLEMENTAL FIGURES

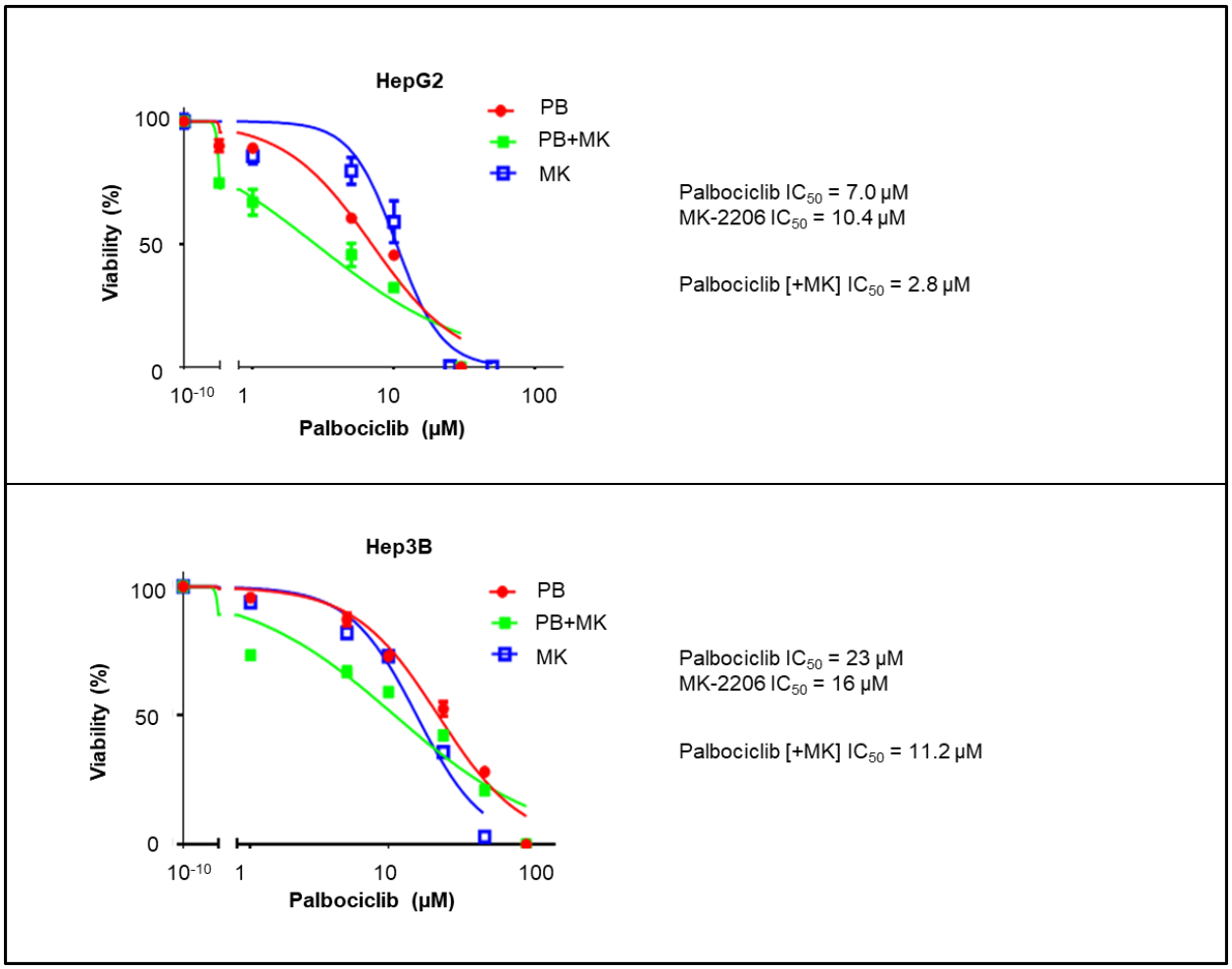

Figure S1: IC50 of palbociclib and MK-2206 IC50 as single agents and in combination. Increasing concentrations of palbociclib (PB) or MK-2206 (MK) were tested to evaluate their IC50 in Hep3B and HepG2 cells. Considering that cell viability of both cell lines was 80% at 5µM MK-2206, we assessed drugs combination using increasing concentrations of palbociclib at a fixed concentration of MK-2206 (5µM). In Hep3B, the combination led to a reduction of palbociclib IC50 to 11.15 µM; in HepG2, to 5 µM. Viability of treated cells were normalized on the average viability of untreated cells. The concentration of drugs [µM] is expressed as a log10 scale. The points represent the average percentage of the viability at each drug concentration and the error bars represent the SD.

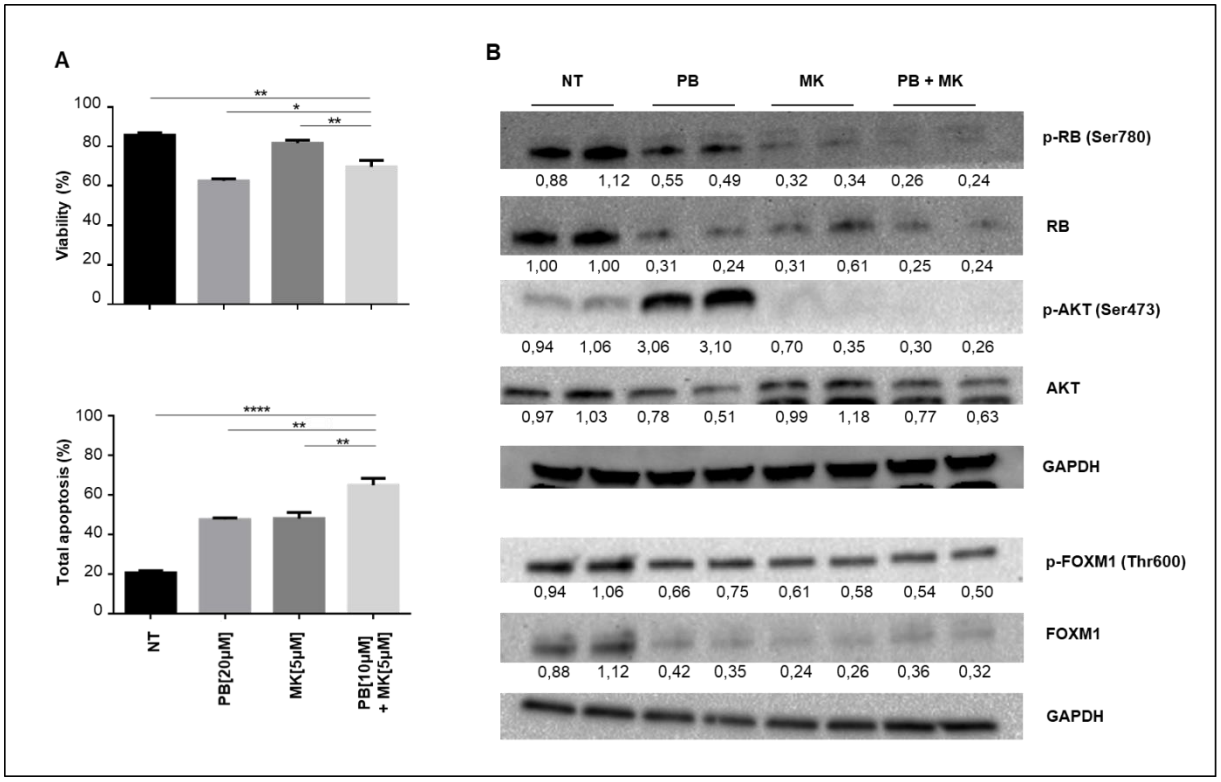

Figure S2. Biological and molecular effects of palbocicib and the AKT inhibitor MK-2206 on Hep3B cells. (A) Hep3B cells were treated with palbocilib (PB) (20µM) or MK-2206 (MK) (5µM) as single agents and with the combination of the two drugs (palbociclib 10uM and MK-2206 5µM). No treatment (NT) was a negative control. Viability and apoptosis were evaluated 72 hours after start of treatment. Data are represented as mean + SD. **(B)** Western blot analysis for quantification of RB1, AKT and FOXM1 proteins and their phosphorylated forms. The values are normalized on GAPDH protein levels and to the average protein levels of the untreated cells (NT). Because Hep3B cells exhibit low level of full length protein, digital images of RB1 and p-RB1 were acquired with an exposure time of 300 seconds instead of 30 sec. *: p value ≤ 0.05; **: p value ≤ 0.01; ***: p value ≤ 0.001; ****: p value ≤ 0.0001

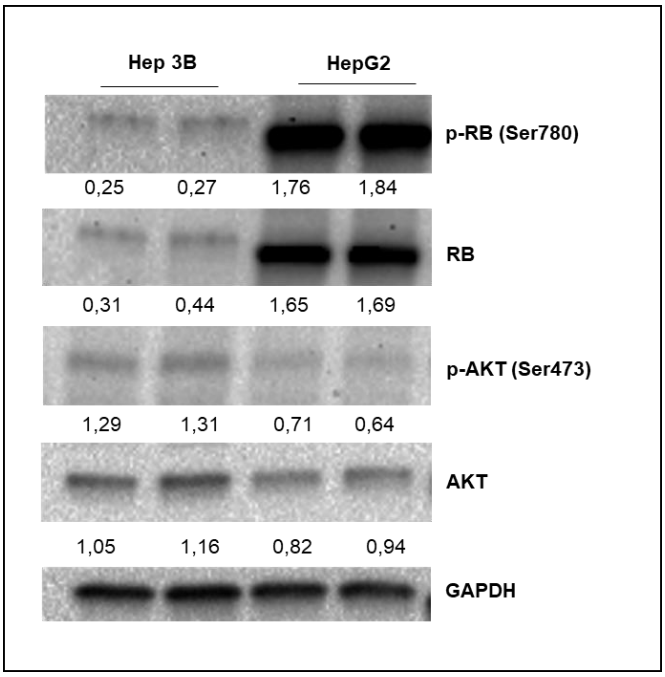

Figure S3. **Basal expression of RB1, AKT proteins in Hep3B and HepG2 cell lines**. Expression of RB1, AKT proteins and their phosphorylated forms was assessed by western blot analysis. The values were normalized on the GAPDH protein levels

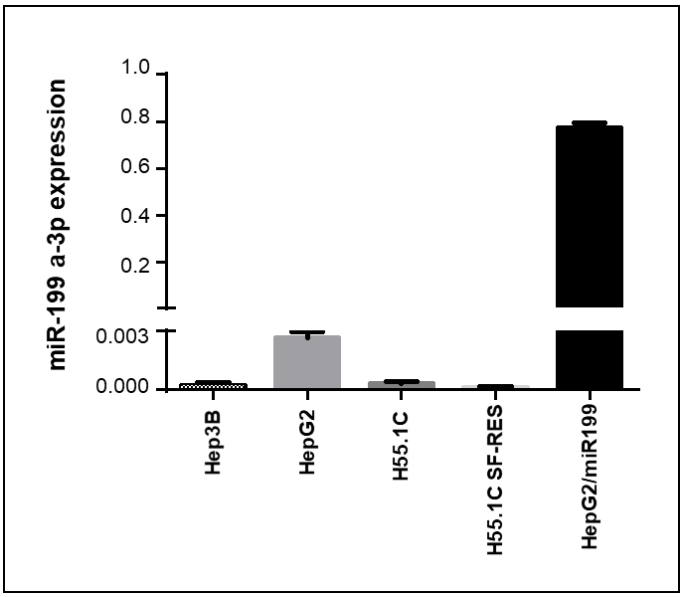

Figure S4. miR-199a-3p expression levels in human and mouse cell lines. Basal levels of miR-199 expression levels were assessed in all the human and mouse cell lines employed in the present study**.** As a positive control for miRNA expression, RNA extracted from HepG2/miR199 cells, a stable cell clone over-expressing miR-199a-3p[1], was included in the analysis. Data are represented as mean + SD.

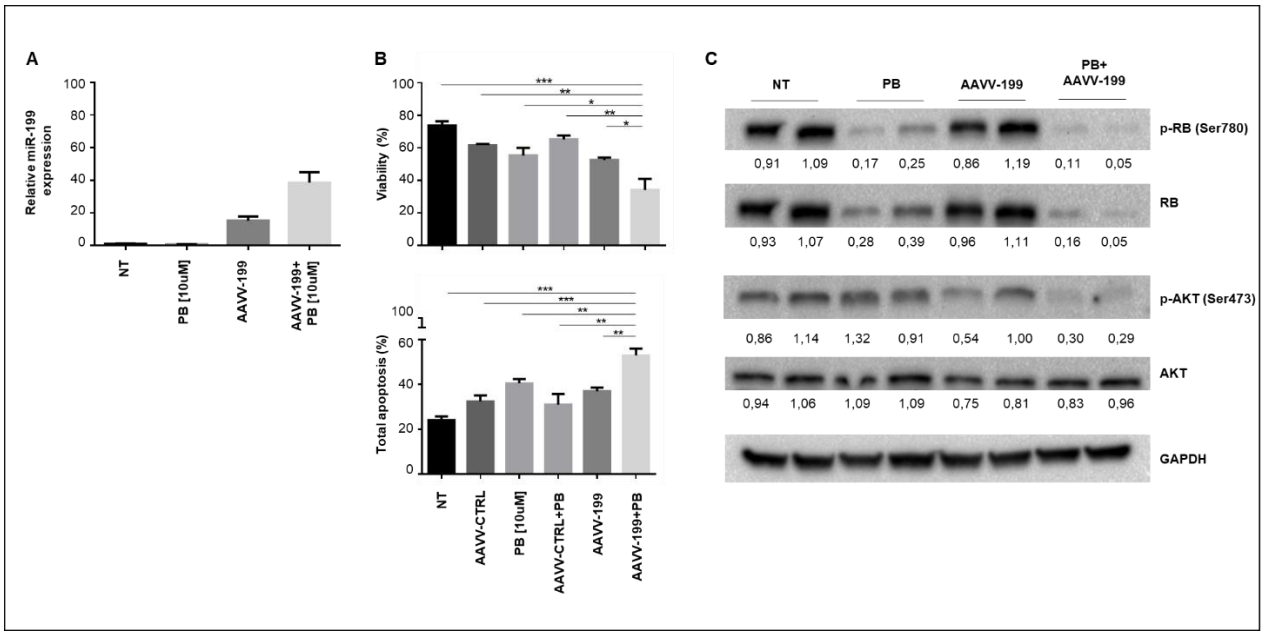

Figure S5. Biological and molecular effects of palbocicib and miR-199a-3p on HepG2 cells. (A) miR-199 expression was measured in HepG2 cells in various conditions: (NT) untreated; (PB 10 uM) palbociclib; (AAVV-199) cells transduced with an Adeno Associated Viral vector expressing miR-199a-3p (MOI=200); (AAVV-199 + PB) combination of AAVV-199 with palbociclib. **(B)** Cells viability and apoptosis levels were evaluated 120h after transduction. Data are represented as mean + SD. **(C)** Western blot analysis and quantification of RB1, AKT proteins by Western blot analysis. The values are normalized on the GAPDH protein and compared to the average levels detected in the untreated cells. *: p value ≤ 0.05; **: p value ≤ 0.01; ***: p value ≤ 0.001; ****: p value ≤ 0.0001.

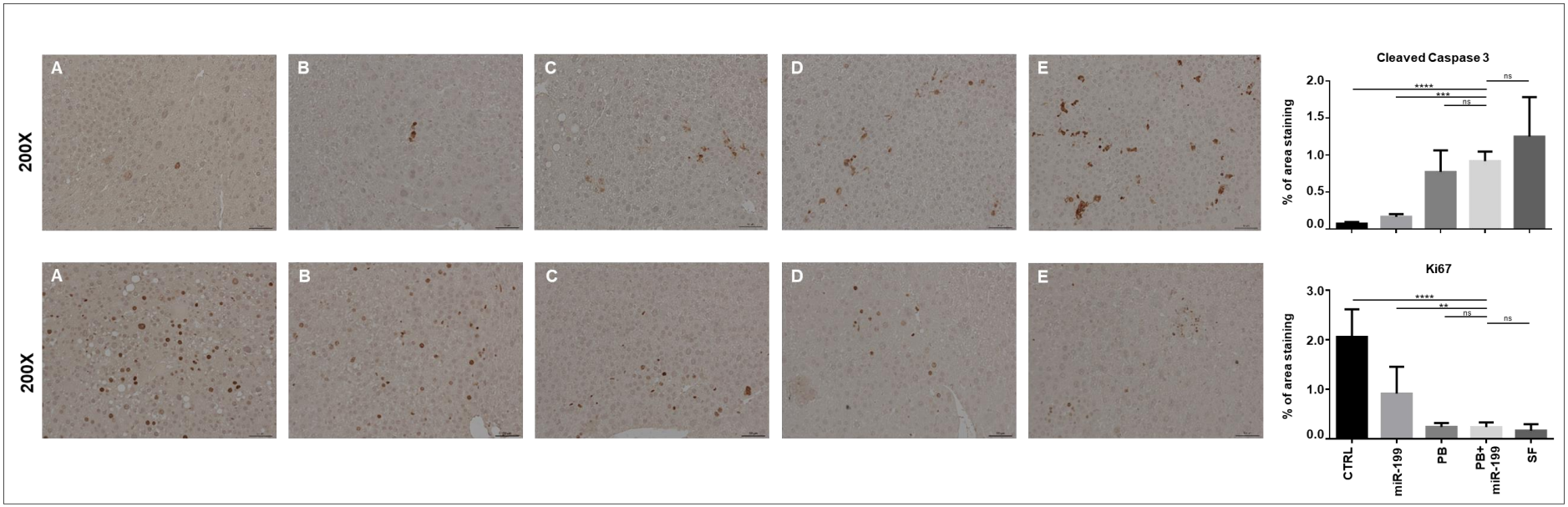

Figure S6: Immunohistochemical analysis of cleaved Caspase-3 (upper panel) and Ki67 (lower panel) in TG221-derived HCC. Each panel is representative of the following experimental conditions: **(A)** CTRL, **(B)** miR-199a-3p, **(C)** Palbociclib, **(D)** Palbociclib+ miR199a-3p, **(E)** Sorafenib. The graphs show the percentage of stained areas for cleaved Caspase-3 or Ki-67 in tissue regions (n = 6) selected for each condition. Magnification 200X, scale bar = 50µm. *: p value ≤ 0.05; **: p value ≤ 0.01; ***: p value ≤ 0.001; ****: p value ≤ 0.0001.

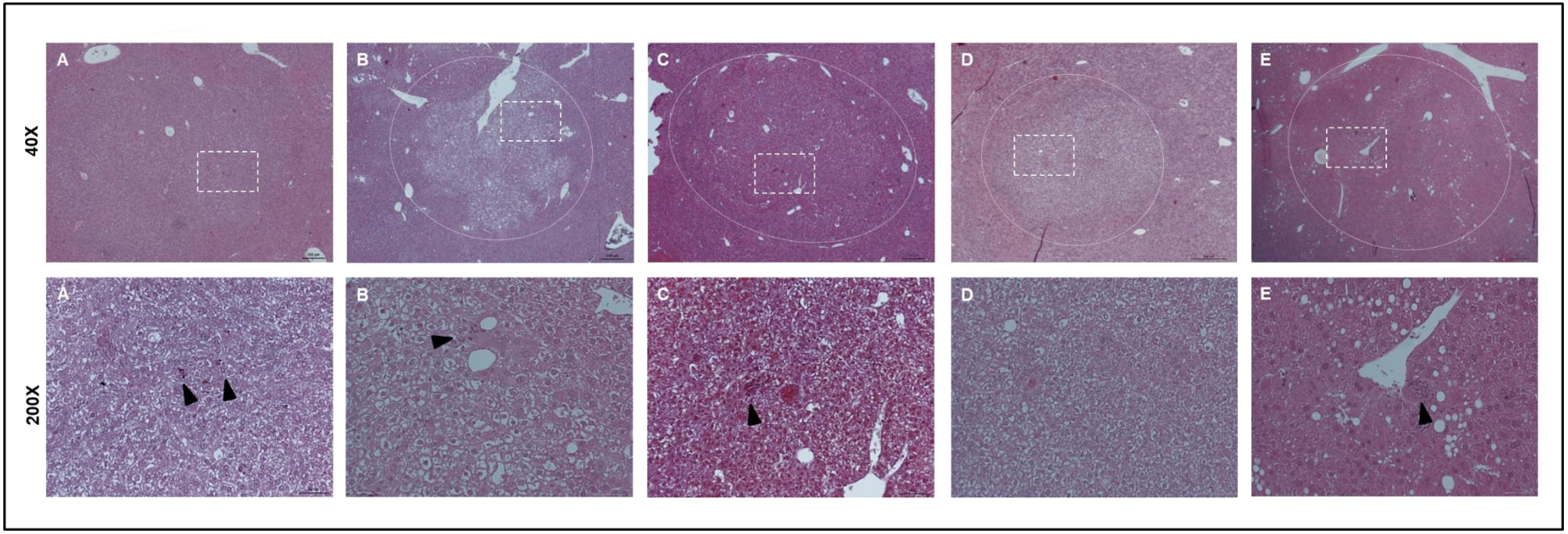

Figure S7. Single drugs or combination treatments do not have a significant impact on the immune response against tumor. Sections derived from the following mice groups: **(A)** CTRL, **(B)** miR-199, **(C)** Palbociclib, **(D)** Palbociclib+ miR199, **(E)** Sorafenib, were stained with hematoxylin-eosin and analysed for the presence of immune and flogistic cell infiltration. Few spots of tumor-infiltrating lymphocytes are indicated by black arrows. Within the 40X magnification images (scale bar = 200µm), circles indicate the tumor nodules and rectangles refers to tissue sections shown in the 200X magnification images (scale bar = 50µm).

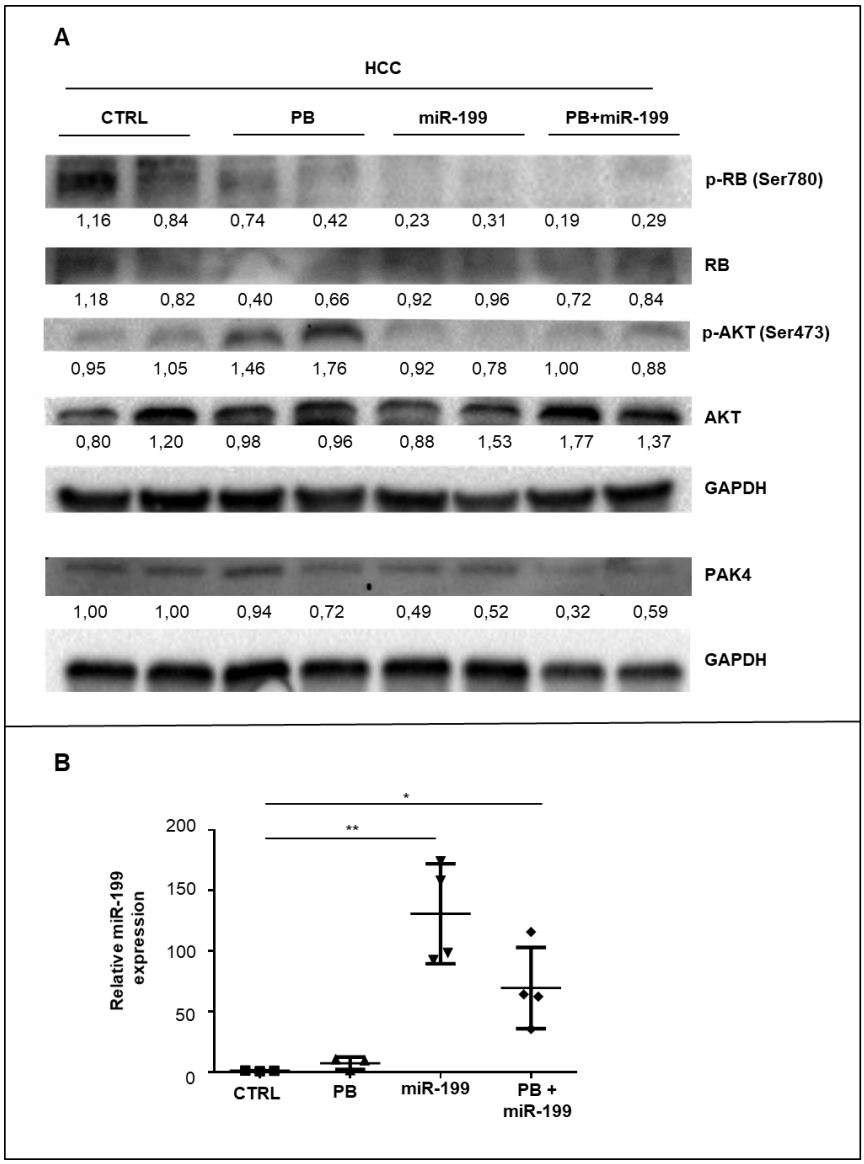

Figure S8. Modulation of palbociclib and miR-199a-3p molecular targets *in vivo*. (A) The expression levels of molecular targets of palbociclib and miR-199a-3p were assessed in HCC samples by Western blot analysis. Each value was normalized on the GAPDH and compared to the average of the untreated (CTRL) samples. **(B)** miR-199 expression levels were evaluated in HCC samples, *: p value ≤ 0.05; **: p value ≤ 0.01; ***: p value ≤ 0.001; ****: p value ≤ 0.0001.

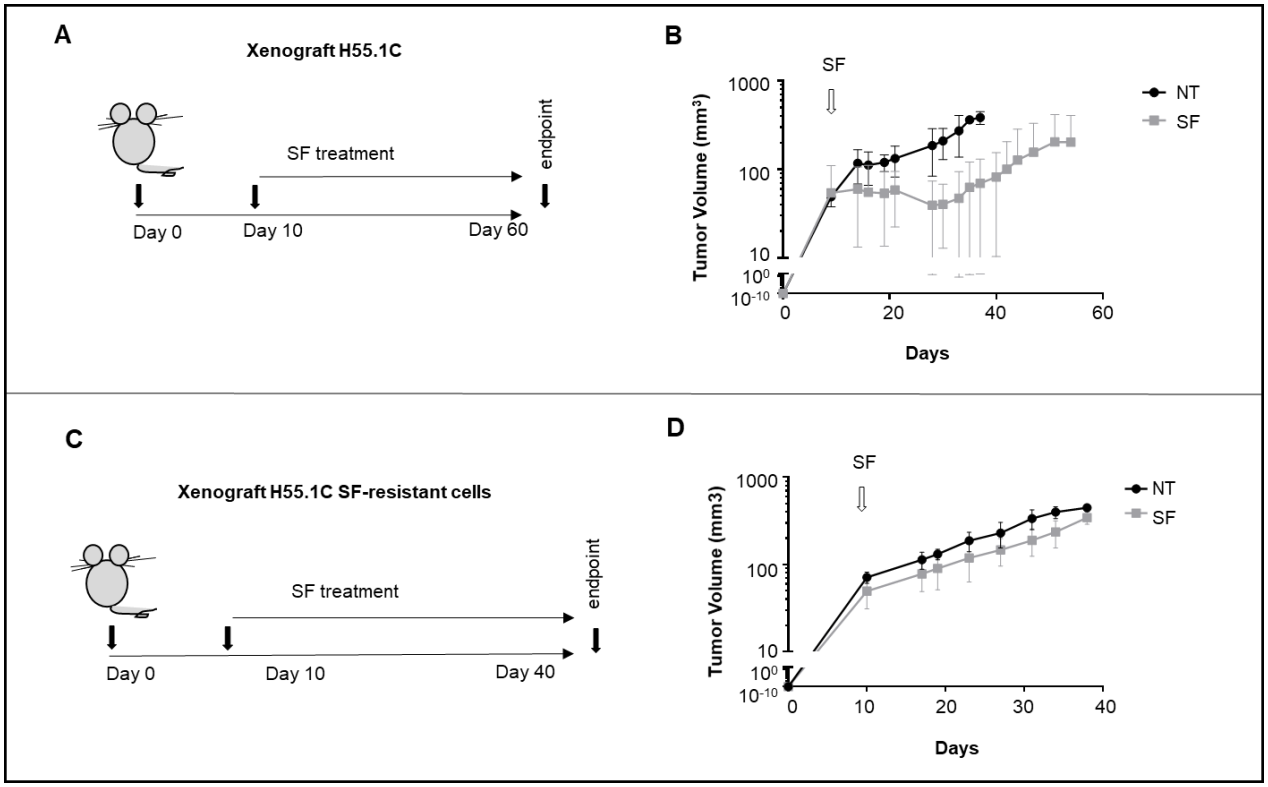

Figure S9. *In vivo* selection of mouse cells resistant to sorafenib. (**A**) H55.1C mouse hepatoma cells were injected subcutaneously into the lateral backside of 8 mice. When tumor reached a volume of ~50 mm^3 (10 days after cells injection), mice were randomly divided into two groups: a group was treated with sorafenib (SF) (n=4), while a second group was not treated (NT) (n=4). **(B**) Size of tumor nodules was measured with a caliper every two days. **(C)** *In vivo* selected SF-resistant cells were injected subcutaneously into the lateral backside of 8 mice. When tumor reached a volume of ~50 mm^3 (10 days after cells injection), mice were randomly divided into two groups: a group was treated with sorafenib (SF) (n=4) for 21 days, while a second group was not treated (NT) (n=4). **(D)** Size of tumor nodules was measured with a caliper every two days. Data are represented as mean ± SD.

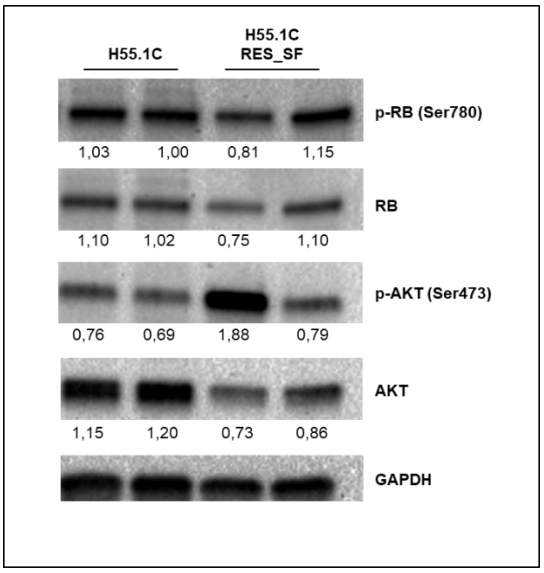

Figure S10. Basal expression of RB1, AKT proteins in H55.1C and H55.1C sorafenib resistant cells. Expression of RB1, AKT proteins and their phosphorylated forms was assessed by western blot analysis. The values were normalized on the GAPDH protein levels

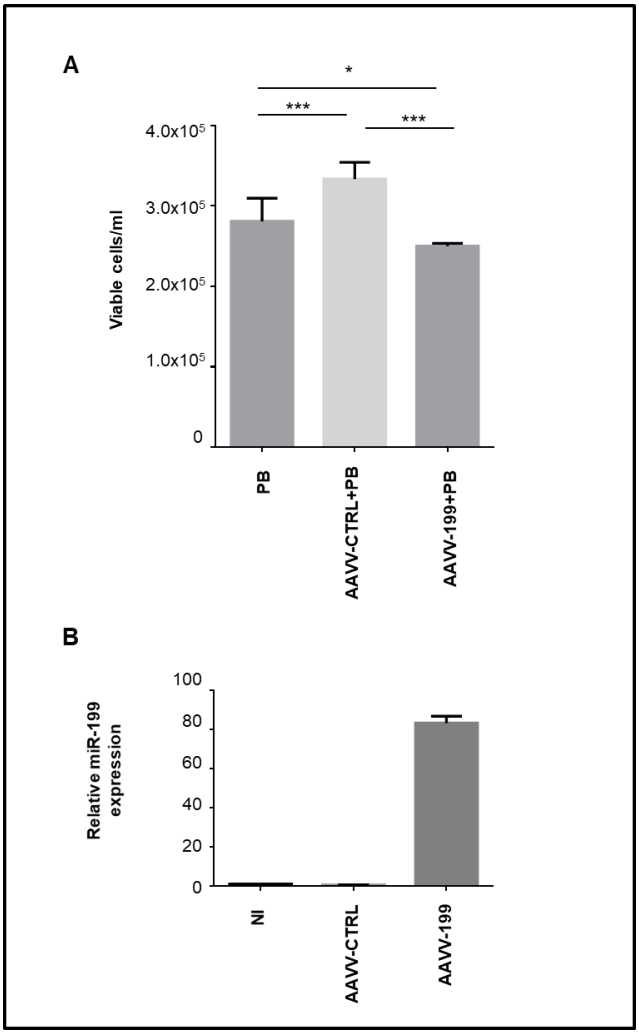

Figure S11. Enforced expression of miR-199a-3p increases palbociclib growth inhibitory effects on sorafenib-resistant HCC mouse cells *in vitro*. Mouse cell lines derived from a SF-resistant tumor (see Figure S9) were infected with an Adeno Associated Virus expressing miR-199a-3p (AAVV-199) or with a control AAVV (AAVV-CTRL) (MOI= 500) and treated with 10 µM palbociclib. At 120h after infection, cells were collected and analyzed. **(A)** Cells treated with miR-199a-3p in combination with palbociclib showed a significant decrease in cell viability compared to single agent treatment. **(B)** miR-199 expression levels were assessed to confirm effective viral vector transduction. Data are represented as mean + SD. *: p value ≤ 0.05; **: p value ≤ 0.01; ***: p value ≤ 0.001; ****: p value ≤ 0.0001.

SUPPLEMENTAL REFERENCES

1. Callegari E, Elamin BK, D'Abundo L, Falzoni S, Donvito G, Moshiri F, Milazzo M, Altavilla G, Giacomelli L, Fornari F, et al. Anti-Tumor Activity of a miR-199-dependent Oncolytic Adenovirus. PLoS One. 2013;8(9):e73964.